CERN-LCGAPP-2004-11

August 15, 2004

In-flight Pion Absorption: Second Benchmark Study for the Validation of Hadronic Physics Simulation at the LHC

Witold Pokorski
CERN

Abstract

We present results on in-flight pion absorption, the second simple benchmark studied in the context of the LCG physics validation project [1]. We compare the data of thin-target experiments to the Geant4 and Fluka simulations. We look at π^+ and π^- beams of energies between 23 MeV and 315 MeV and targets made of Al, Cu and Au. We find that the simulations show a generally good agreement with the experimental data, although very precise comparison cannot be made due to large uncertainties on the experimental data.

1 Introduction

The validation for the full detector response simulation of the Monte Carlo programs like Fluka [3] or toolkits like Geant4 [2] is usually performed using test beam data. In such cases the simulation application consists of (often very complex) test-beam geometries and 'particle guns' as sources of incident particles. The results are then validated (that is, compared to the experimental data) at the macroscopic level, i.e. by looking at the output of a given subdetector which reflects a large number of different processes combined together. In addition to the test-beam validation, one can also check individual processes implemented in the simulation engines on a microscopic basis by performing simulation of single particle-nucleus interactions. In this paper we describe one of such benchmarks in which we study the in-flight pion absorption.

2 Experimental data

In order to study individual pion-nucleus interactions, thin target experiments have been considered. The purpose of having a thin target (i.e. much smaller than the interaction length) is to avoid multiple interactions, in other words to allow the products of the original pion-nucleus interaction to reach the detector unaffected. Most of the incident particles traverse the target without interacting, but some of them undergo a single interaction, which allows us to study the pion absorption process.

Unfortunately, there exists very few experimental results from thin target experiments for total pion absorption cross-section in the literature. The only two documented experiments are those by Ashery et al. [4] and by Nakai et al. [5]. In addition, that data is affected by quite big uncertainties.

3 Simulation setup

As we mentioned in the previous section, in thin target experiments most of the incident particles traverse the target without interacting. The interesting events, i.e. those where an inelastic process takes place, are rather rare. Therefore, to speed up the generation of data, we do not simulate the actual geometry, but we use some technical tricks.

For the Geant4 simulation, we used as starting point the code developed for a similar kind of studies in the context of the Alice experiment [7] by I. Gonzalez [6]. The approach consists of simulating a very large block of material with all processes, except transportation and inelastic scattering, switched off. With such settings, the particle is transported in the block of material until the inelastic process takes place. At that point, the tracking is stopped and only the information concerning the products of the reaction is stored. For our studies we used the QGSP_BERT 1.2 physics list [8], where the classical Bertini cascade [9] is used for nucleon and pion induced reactions below 3 GeV kinetic energy.

We use a similar kind of approach for the Fluka simulation. Instead of describing the real geometry (which would make the simulation very slow), we use a 'by-pass' [10] to directly call the process we are interested in and to examine the outgoing particles. The version of Fluka that was used for the study was 2003.1.

4 Results

The first set of plots in Figures 1-6 shows the total reaction (non-elastic) cross sections. The simulations results (Geant4 and Fluka) were obtained from samples of 200000 events. In the case of the Geant4 simulation, the cross section data is based on the Barashenkov systematics [9], while in the case of Fluka, the cross section is calculated using the Fluka-internal theoretical model [3]. In addition, we also plot the experimental values listed in the paper by Ashery et al. [4]. As we can see from these plots, simulation and data show a reasonable agreement. It can also be noted that the agreement is better for lighter nuclei.

The main purpose of the benchmark is to study the absorptive part of the reaction cross section. If we write, therefore,

$$\sigma_{abs} = r * \sigma_{react} \tag{1}$$

where σ_{react} is the total reaction cross section and σ_{abs} is the absorption cross section, the factor r gives the fraction of events where there are no outgoing pions. The plots on Figures 7-12 show the factor r for the different materials. We can see that Fluka and Geant4 in general show a similar behavior and that the discrepancies are the largest for high energy beams on light materials. Due to the lack of experimental results, however, we cannot conclude which package gives the best prediction.

In order to compare with the experimental data, in Figures 13-18 we plot the absorption cross-section σ_{abs}. We observe that in some cases the experimental data coming from the two different sources ([4] and [5]) show large discrepancies. This indicates that one cannot make very precise comparison with the simulation. However, the general agreement is good, with the Fluka points slightly closer to the experimental data than the Geant4 ones. What is also interesting is that Fluka and Geant4 exhibit the best agreement with each other for 'medium-weight' materials, while they show discrepancies both for light materials (where the Geant4 absorption cross sections are in general smaller than the Fluka ones) and for heavy materials (where the Geant4 absorption cross sections are in general larger than the Fluka ones). Figures 19-30 show the same results but this time in the form of the ratio of simulated to experimental data for both the Nakai[5] and the Ashery[4] data. In order to be able to study the level of agreement more quantitatively, in Figures 31-42 we show the simulated to experimental ratio distribution weighted with weights being $\exp(-err)$ where err are the experimental errors as in Figures 19-30. Those plots confirm our observation made at the beginning of the paragraph, showing that the mean ratio for Fluka is in most of the cases closer to 1 (and the RMS smaller).

The final set of plots in Figures 43-48 and in Figures 49-54 show the type multiplicity of the outgoing particles after the reaction as well as the multiplicity of the outgoing pions as function of energy. These multiplicities are consistent with the expectations. For instance in the case of the beam of π^-, most of the outgoing pions is also of the type π^- (due to the inelastic scattering of the incoming pions), there is some number of π^0 (due to the charge exchange of the incoming pions) and finally there is the smallest number of π^+ (due to the double charge exchange of the incoming pions). Moreover, the sum of the average number of the different types of outgoing pions per event is less than one, which reflects the fact that sometimes pion absorption takes place, i.e. there is no pion among the outgoing particles. The average numbers of the different types of outgoing pions corresponds to the probabilities of the different processes to occur. Concerning the comparison between Fluka and Geant4, the particle multiplicities are quite similar. The only significant difference is in the average number of photons per event, which is probably due to different models of the generation of low energy photons after the reaction, and which has no impact on the studies presented here.

5 Conclusions

The second simple benchmark study performed in the context of the LCG Physics Validation addressed pion absorption in-flight. We have compared the simulation results from Geant4 and Fluka with thin target experiments described in the literature. The latter consisted of beams of pions (π^+ and π^-) of energies between 23 MeV and 315 MeV on targets made of Al, Cu and Au.

The results show a generally good agreement between both simulation packages and the experimental data. In most of the cases the Fluka points are closer to those coming from the experiments, but in some of the cases the Geant4 ones seem to agree better. Unfortunately, due to large uncertainties in the data, precise comparisons are not possible. Geant4 and Fluka agree better with each other for intermediate weight materials like Cu. The discrepancies become larger for light materials like Al and for the heavy materials like Au. On the other hand, the multiplicity and type of the outgoing particles are qualitatively similar.

The author would like to thank John Apostolakis, Federico Carminati, Alfredo Ferrari, Fabiola Gianotti, Mikhail Kosov, Paola Sala, Johannes Peter Wellisch and Juerg Beringer for many useful discussions and suggestions.

This work received support from Particle Physics and Astronomy Research Council, Swindon, UK.

References

[1] http://lcgapp.cern.ch/project/simu/validation/

[2] http://wwwasd.web.cern.ch/wwwasd/geant4/geant4.html

[3] http://www.fluka.org/

[4] D. Ashery et al., Phys.Rev.C, Vol. 23, 2173 (1981)

[5] K. Nakai et al., Phys.Rev.Lett., Vol. 44, 1446 (1980)

[6] http://i.home.cern.ch/i/iglez/www/alice/HadTests/

[7] http://alice.web.cern.ch/Alice/AliceNew/

[8] http://wwwasd.web.cern.ch/wwwasd/geant4/geant4.html

[9] A. Heikkinen, N. Stepanov and J.-P. Wellisch, “Bertini intra-nuclear cascade implementation in Geant4”, CHEP2003 conference proceedings

[10] A. Ferrari, private communication

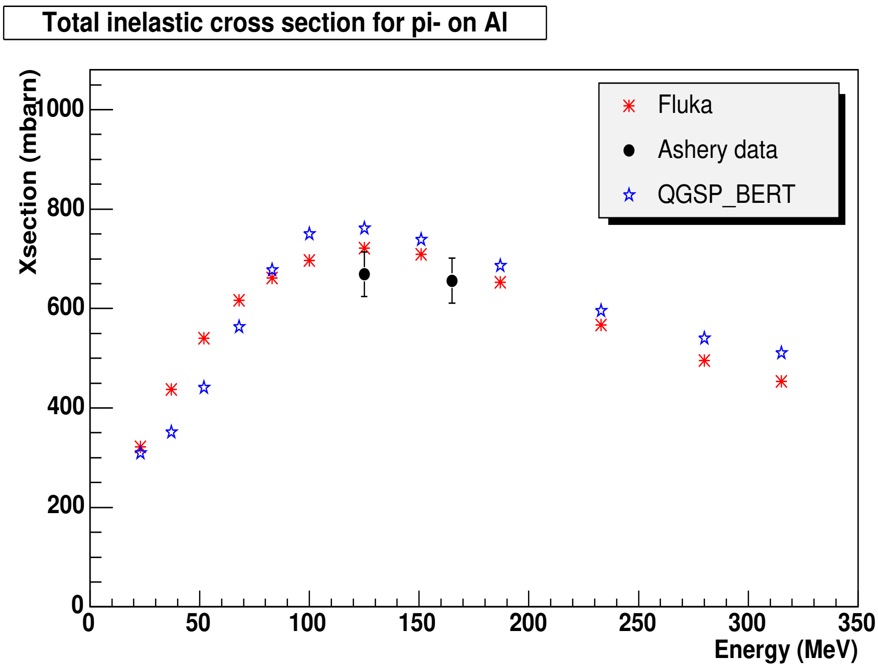

Figure 1: Total inelastic cross section for π^- on aluminium as a function of energy

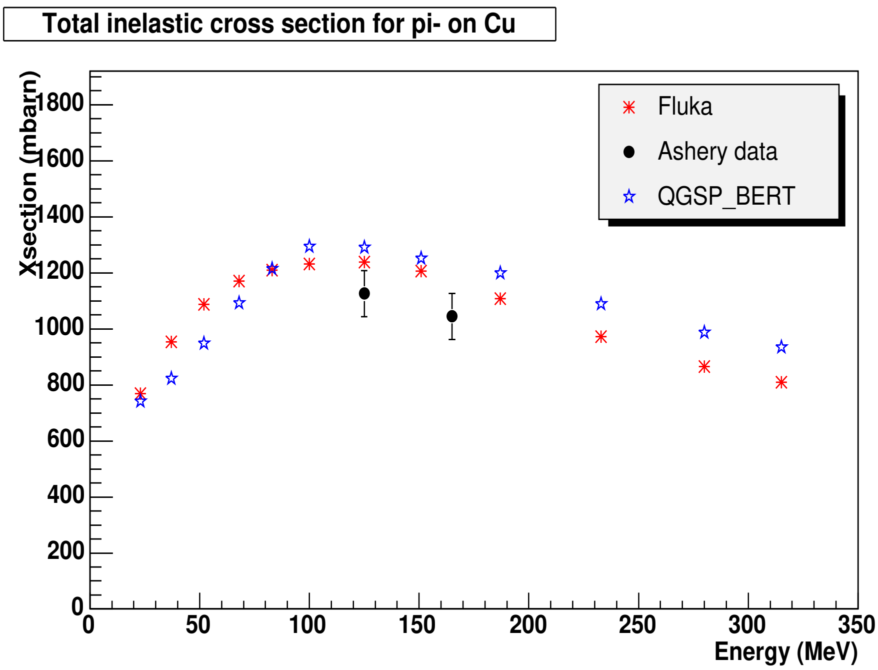

Figure 2: Total inelastic cross section for π^- on copper as a function of energy

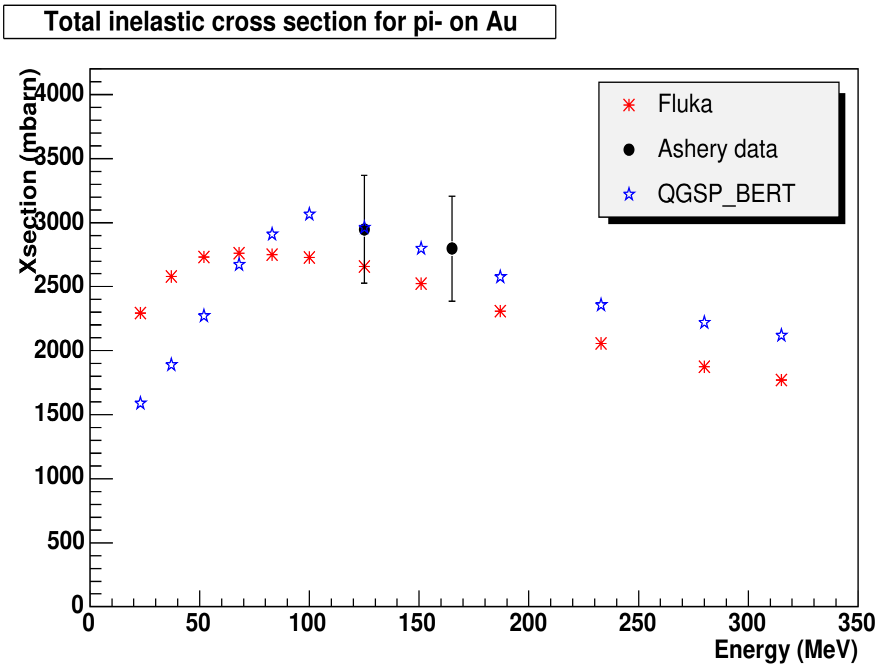

Figure 3: Total inelastic cross section for π^- on gold as a function of energy

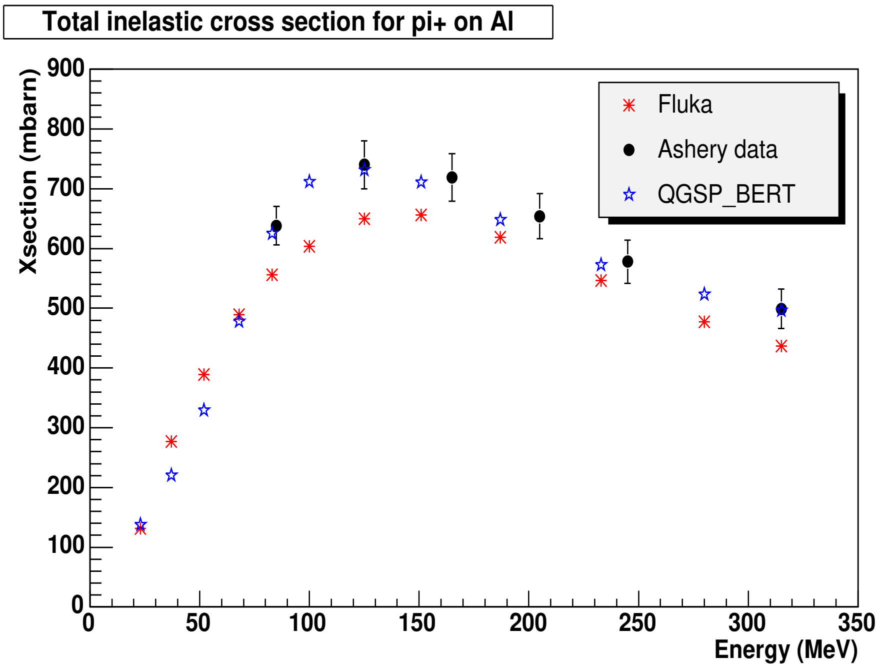

Figure 4: Total inelastic cross section for π^+ on aluminium as a function of energy

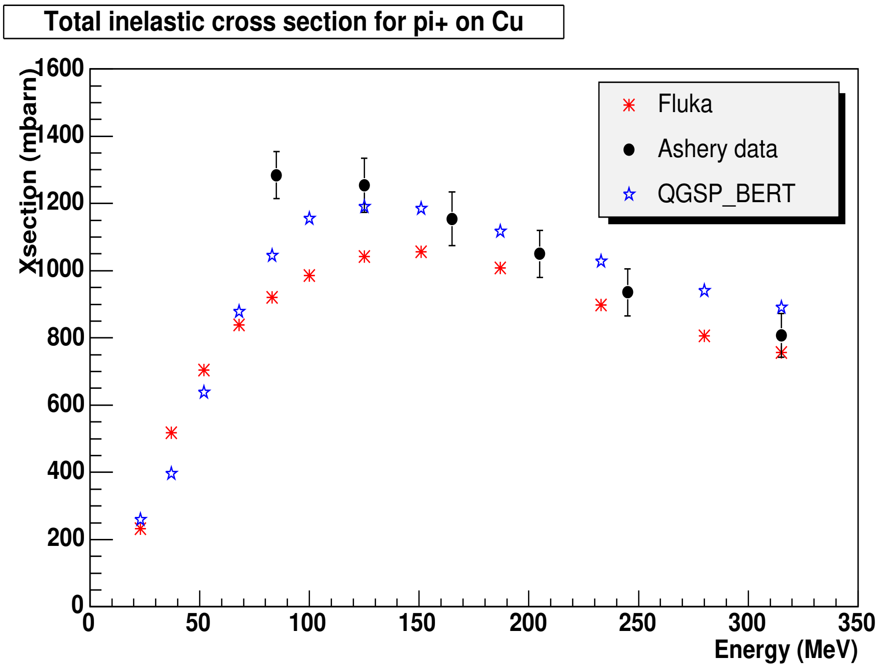

Figure 5: Total inelastic cross section for π^+ on copper as a function of energy

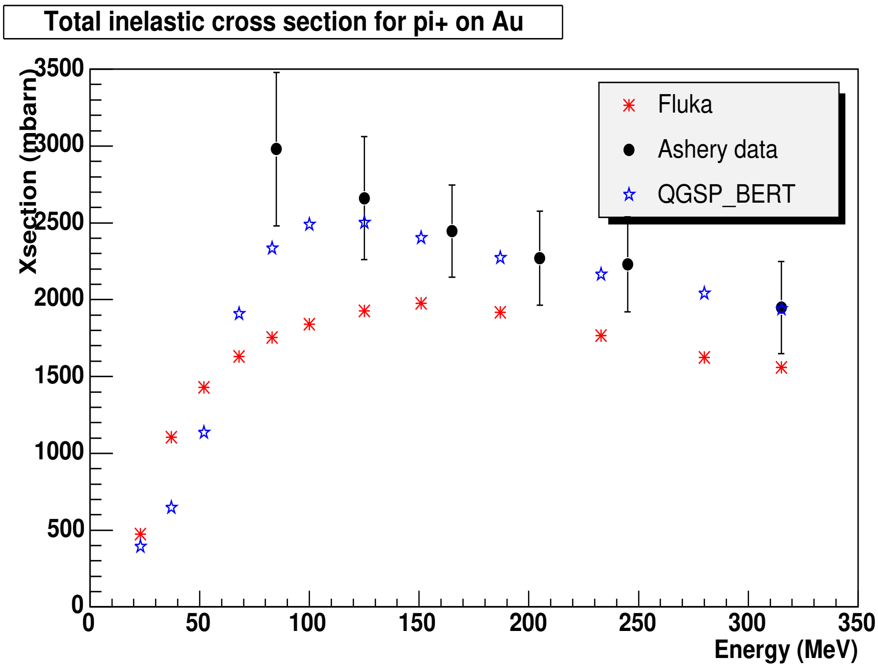

Figure 6: Total inelastic cross section for π^+ on gold as a function of energy

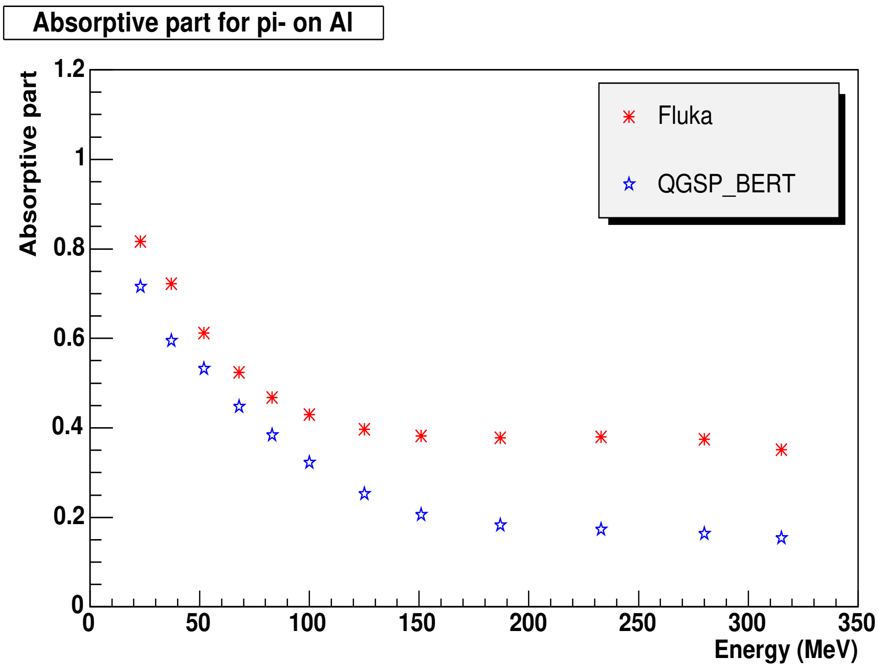

Figure 7: Absorptive part of the non-elastic cross-section for π^- on aluminium as a function of energy

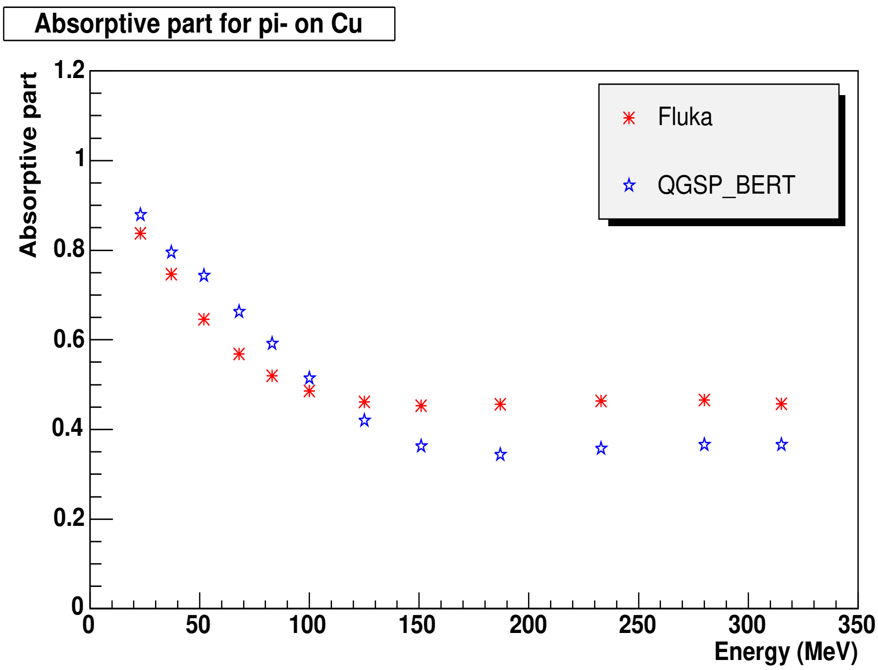

Figure 8: Absorptive part of the non-elastic cross-section for π^- on copper as a function of energy

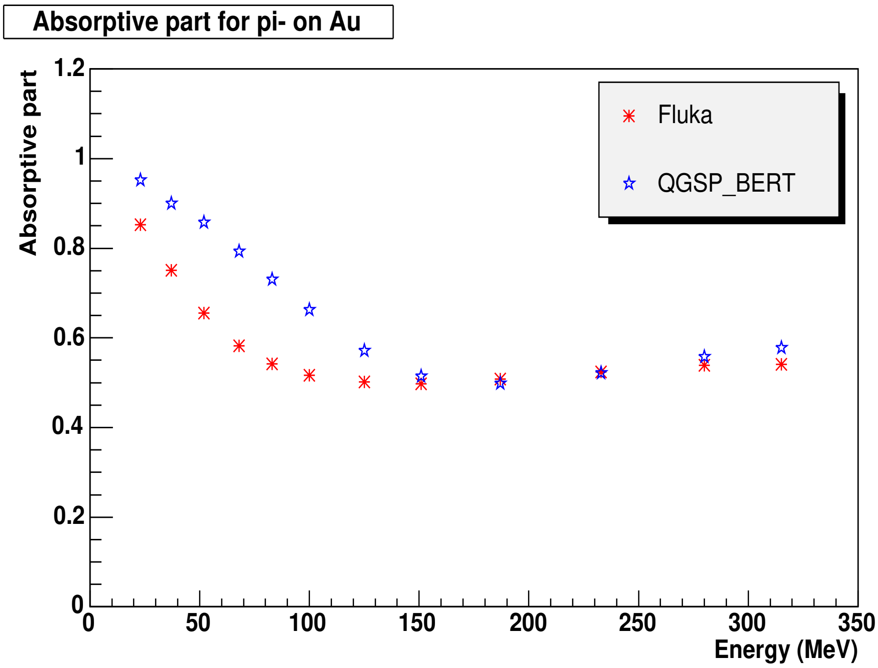

Figure 9: Absorptive part of the non-elastic cross-section for π^- on gold as a function of energy

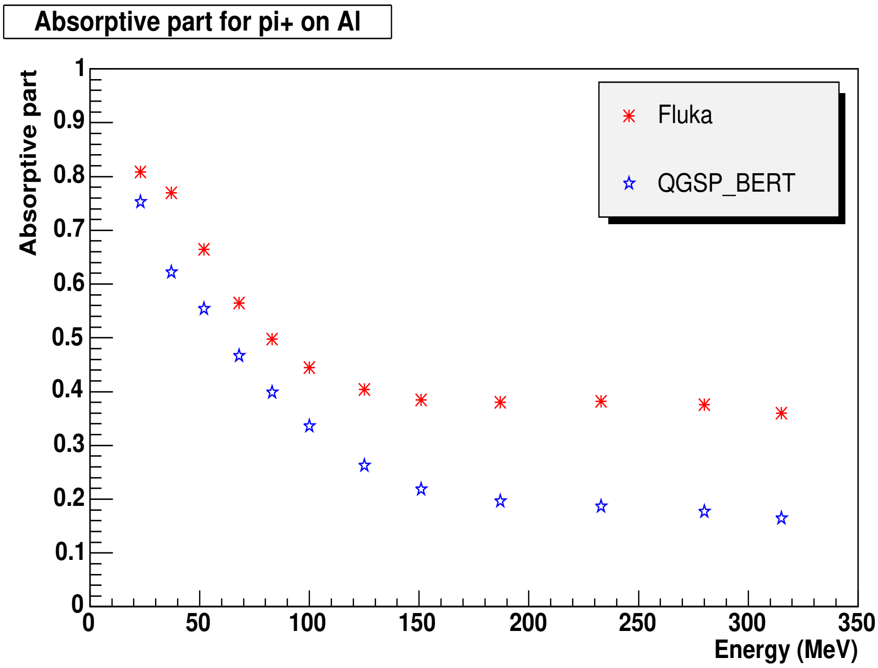

Figure 10: Absorptive part of the non-elastic cross-section for π^+ on aluminium as a function of energy

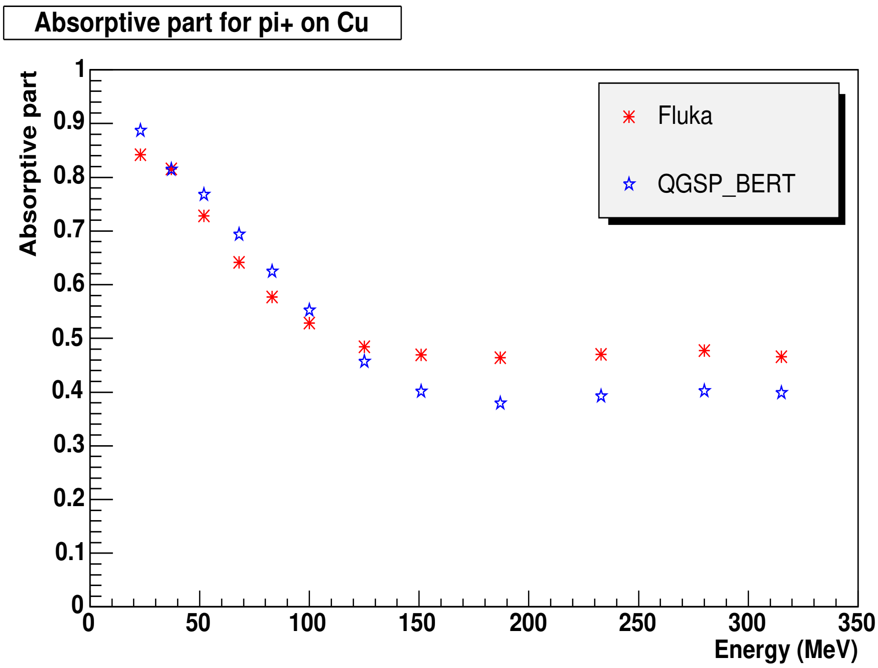

Figure 11: Absorptive part of the non-elastic cross-section for π^+ on copper as a function of energy

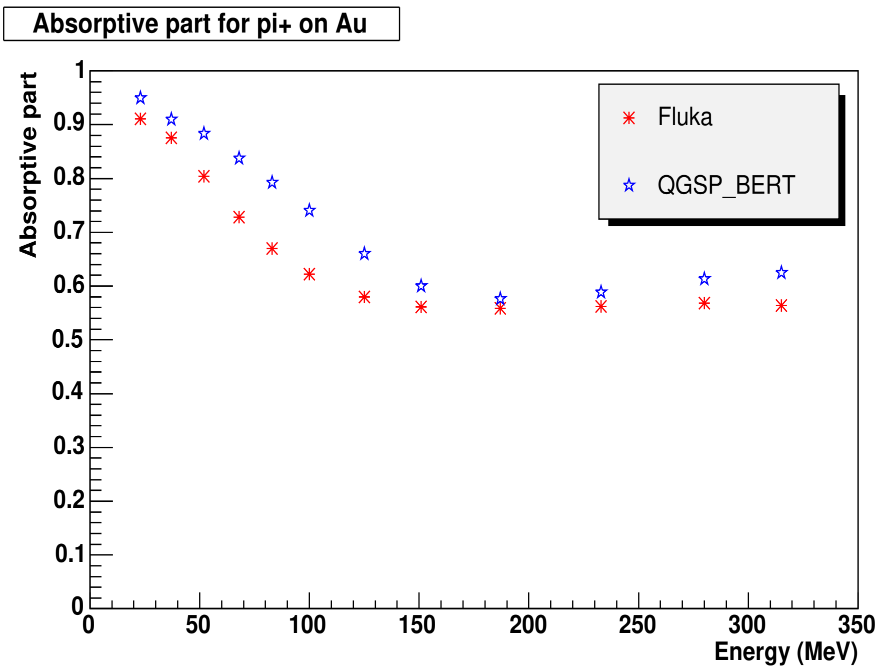

Figure 12: Absorptive part of the non-elastic cross-section for π^+ on gold as a function of energy

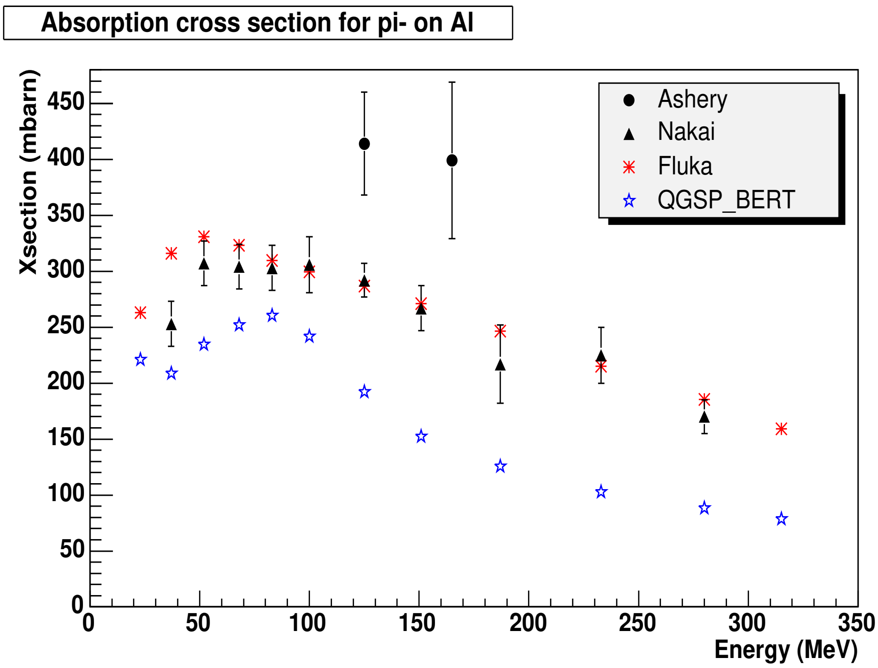

Figure 13: Total absorption cross section for π^- on aluminium as a function of energy

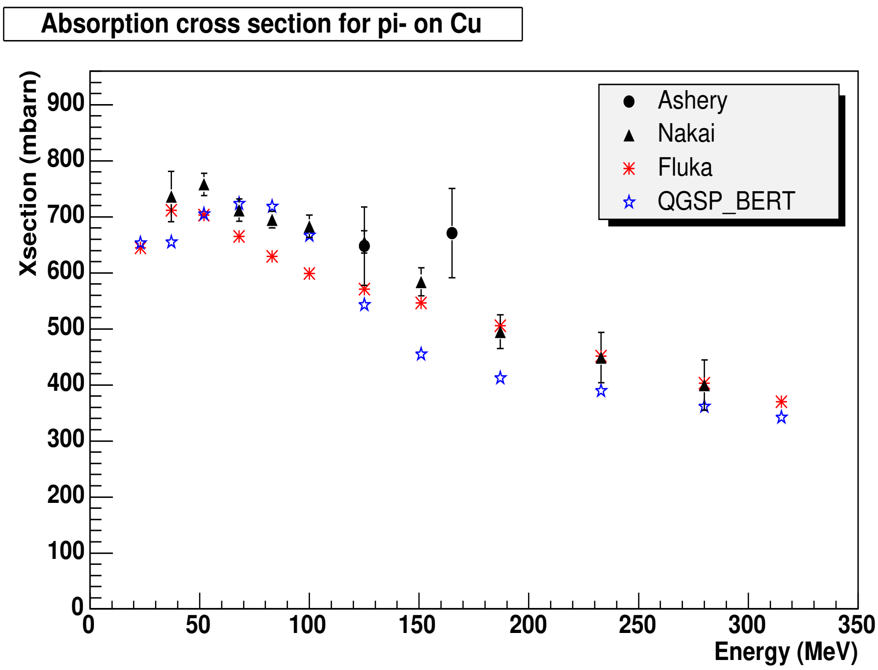

Figure 14: Total absorption cross section for π^- on copper as a function of energy

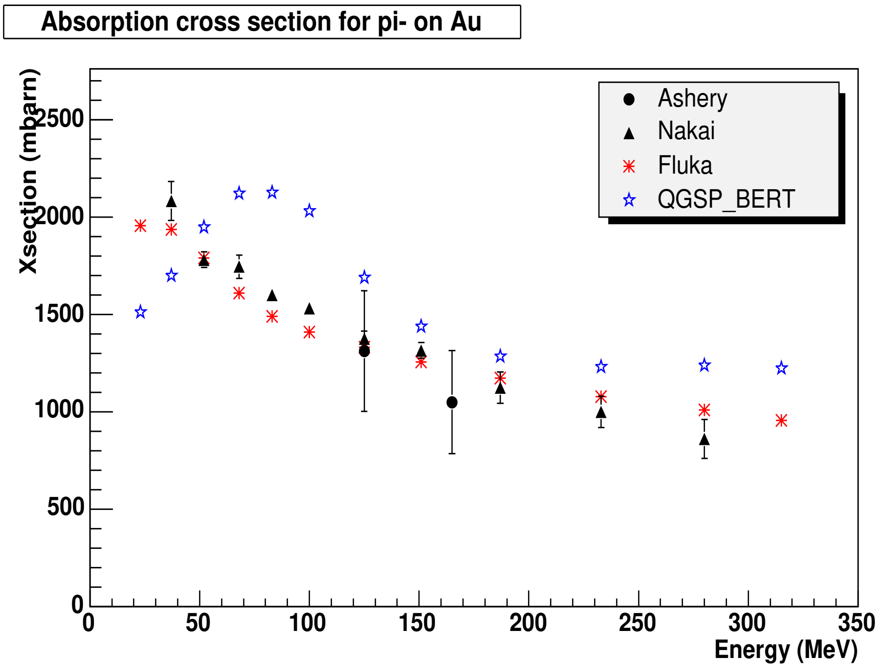

Figure 15: Total absorption cross section for π^- on gold as a function of energy

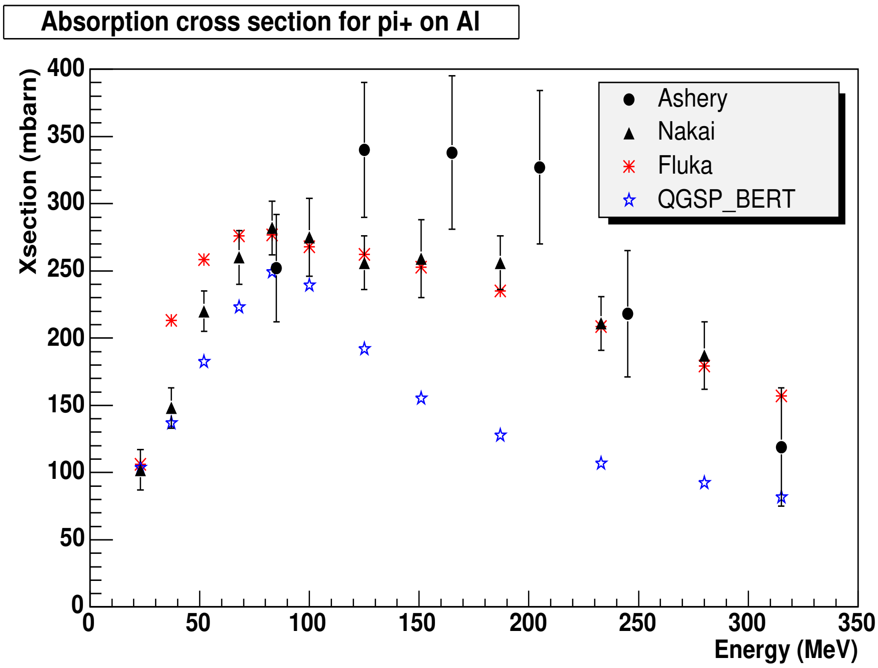

Figure 16: Total absorption cross section for π^+ on aluminium as a function of energy

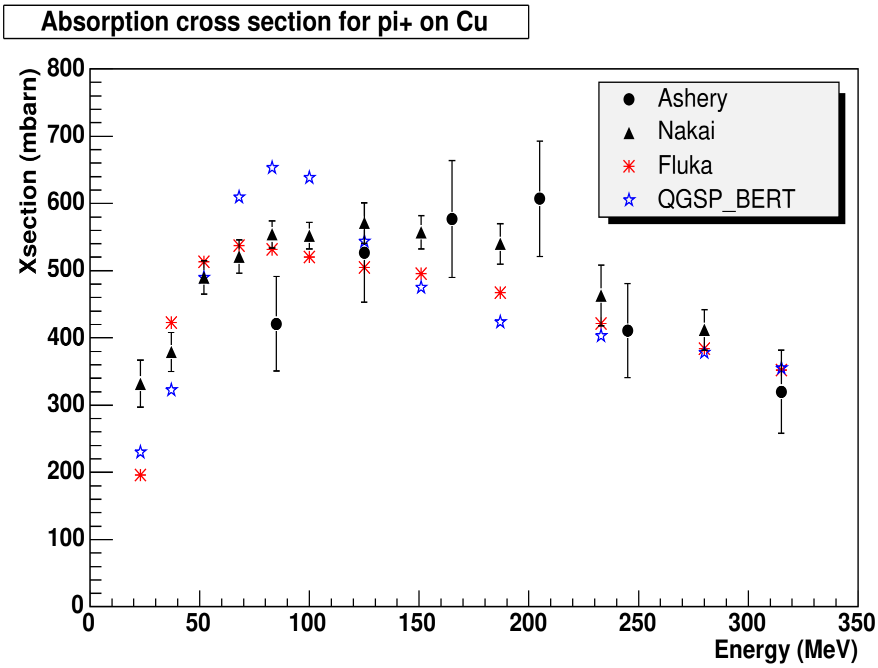

Figure 17: Total absorption cross section for π^+ on copper as a function of energy

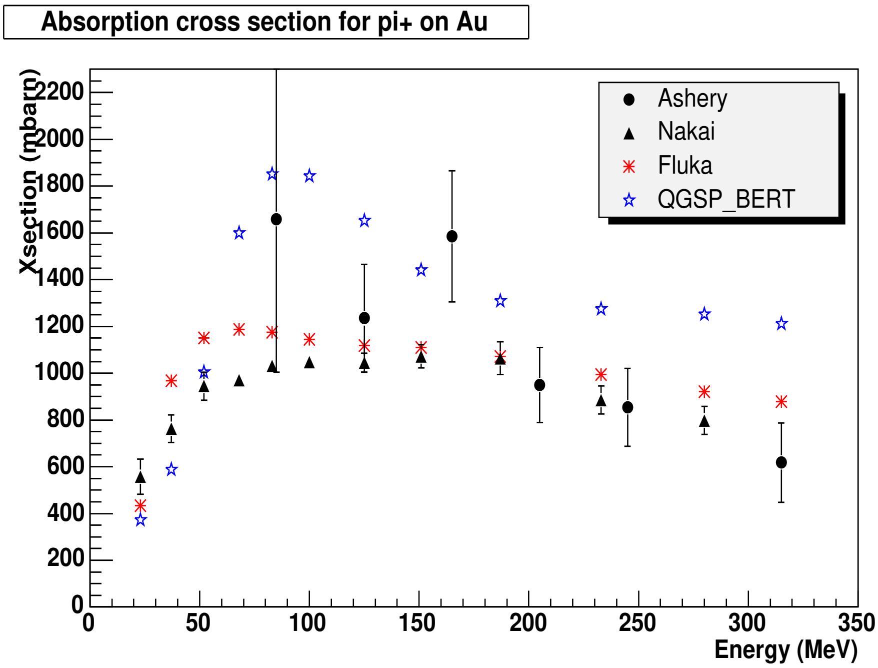

Figure 18: Total absorption cross section for π^+ on gold as a function of energy

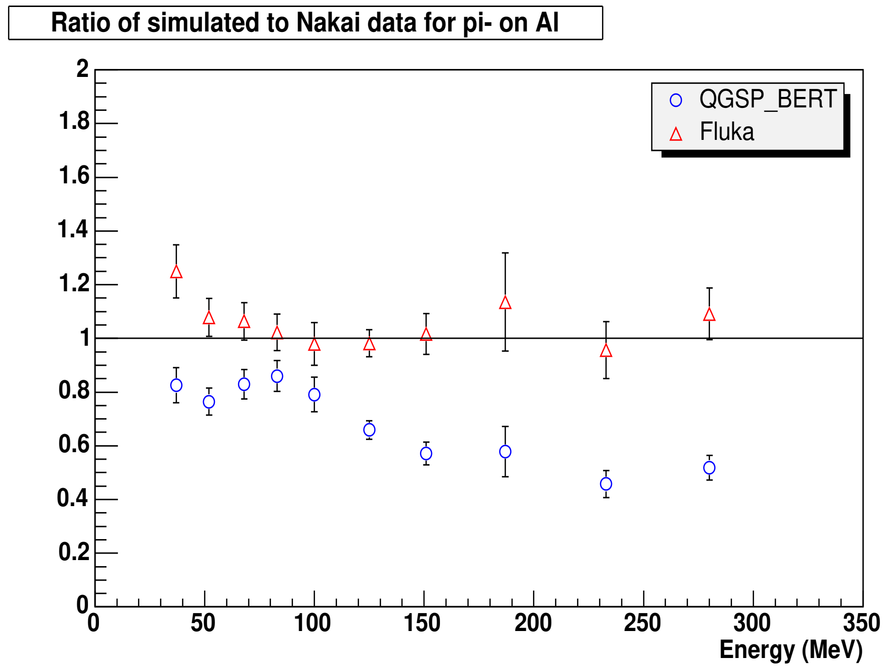

Figure 19: Simulated to experimental (Nakai) total absorption cross section ratio for π^- on aluminium as a function of energy

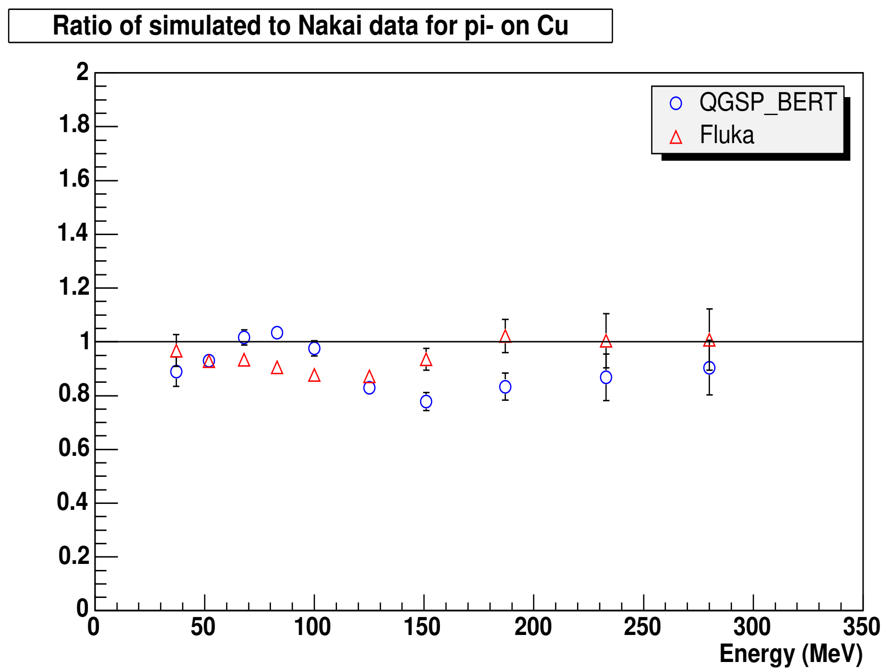

Figure 20: Simulated to experimental (Nakai) total absorption cross section ratio for π^- on copper as a function of energy

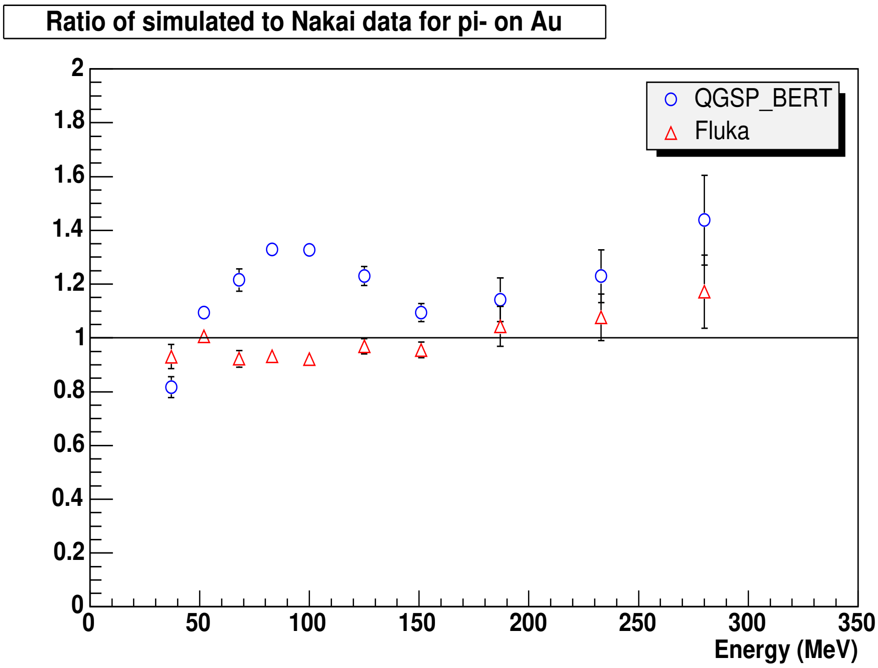

Figure 21: Simulated to experimental (Nakai) total absorption cross section ratio for π^- on gold as a function of energy

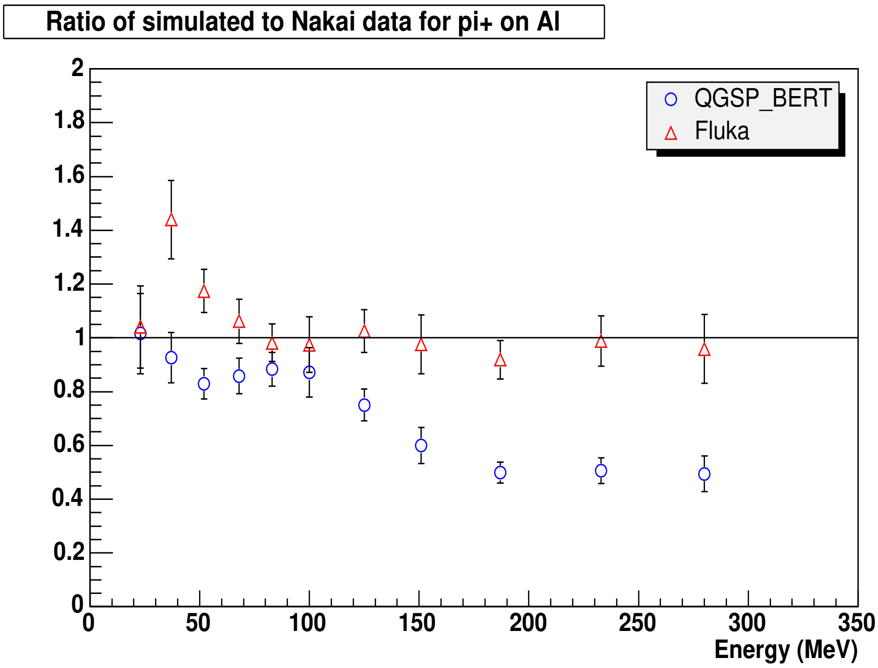

Figure 22: Simulated to experimental (Nakai) total absorption cross section ratio for π^+ on aluminium as a function of energy

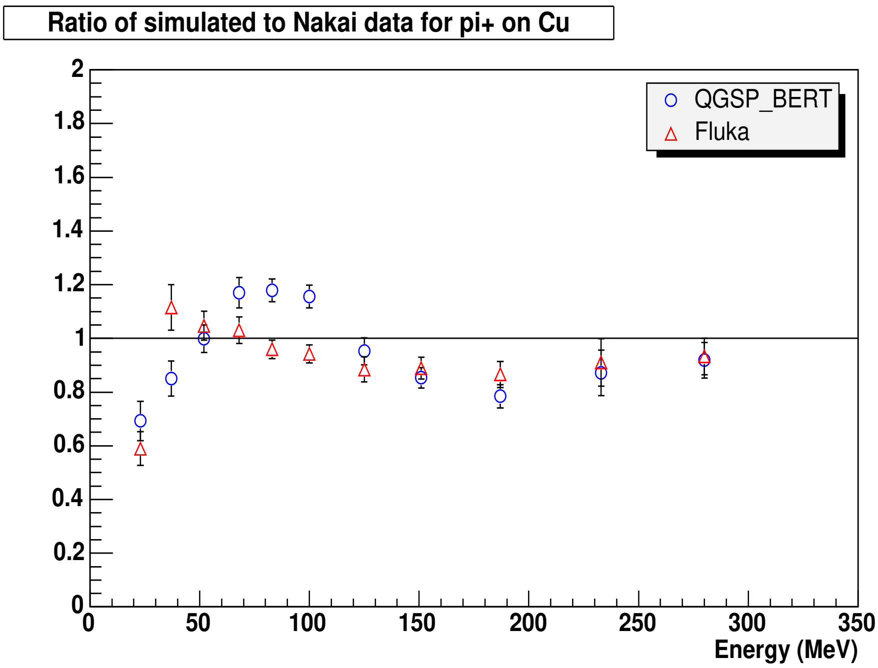

Figure 23: Simulated to experimental (Nakai) total absorption cross section ratio for π^+ on copper as a function of energy

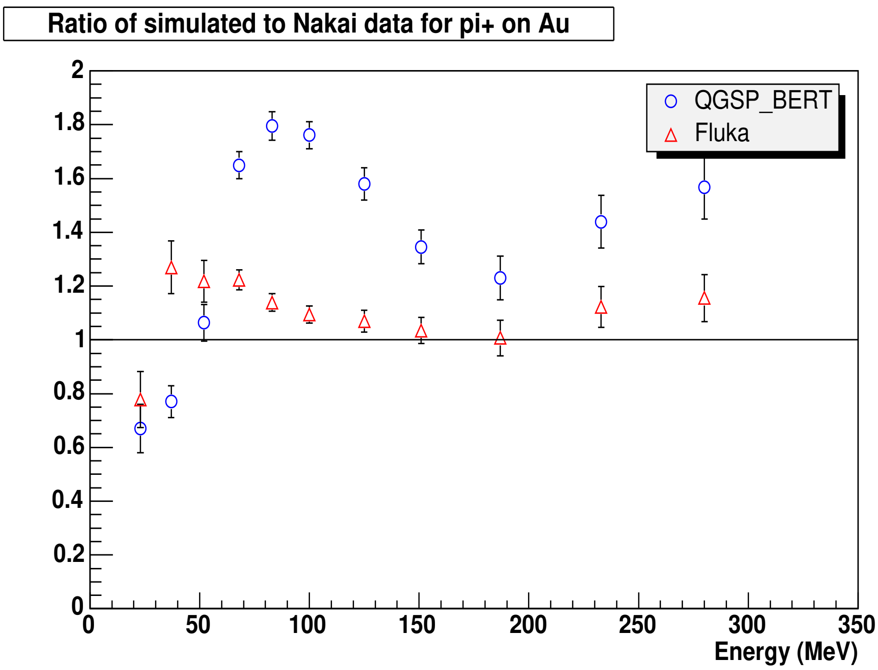

Figure 24: Simulated to experimental (Nakai) total absorption cross section ratio for π^+ on gold as a function of energy

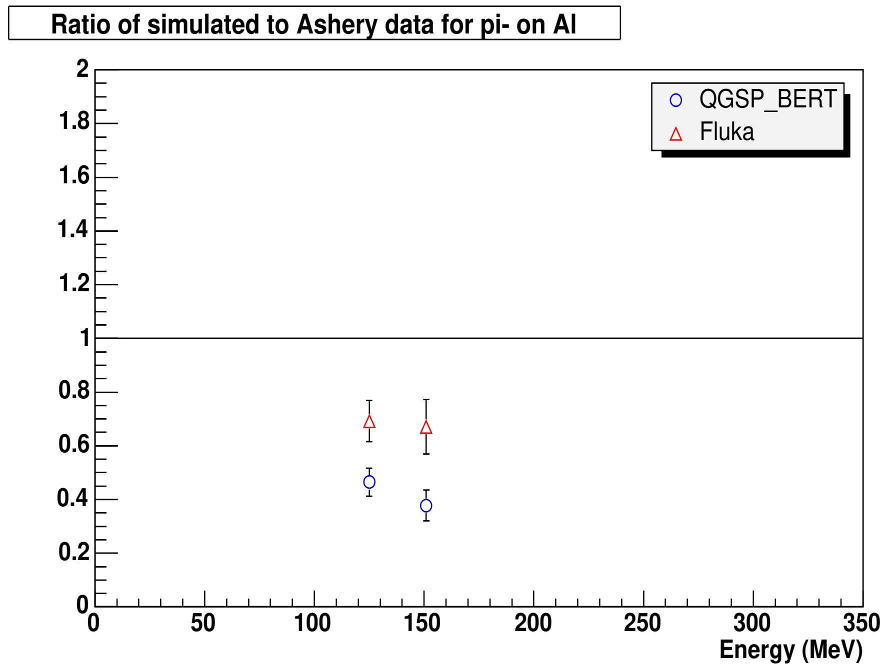

Figure 25: Simulated to experimental (Ashery) total absorption cross section ratio for π^- on aluminium as a function of energy

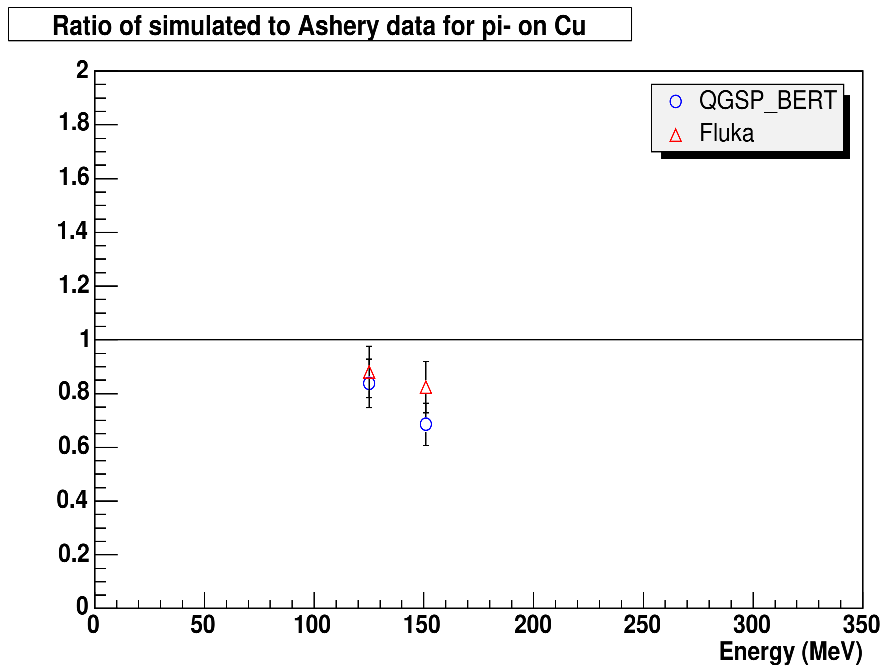

Figure 26: Simulated to experimental (Ashery) total absorption cross section ratio for π^- on copper as a function of energy

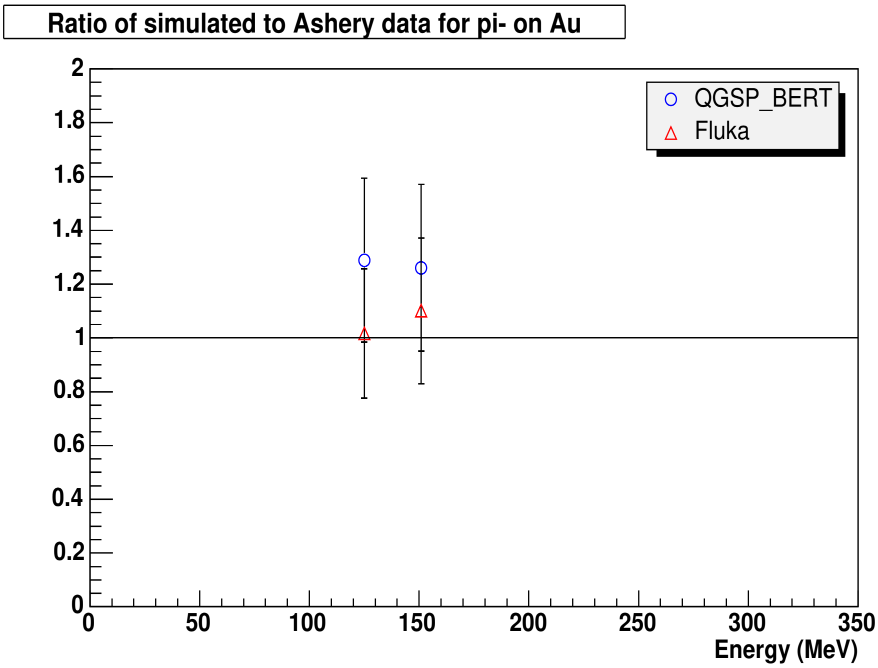

Figure 27: Simulated to experimental (Ashery) total absorption cross section ratio for π^- on gold as a function of energy

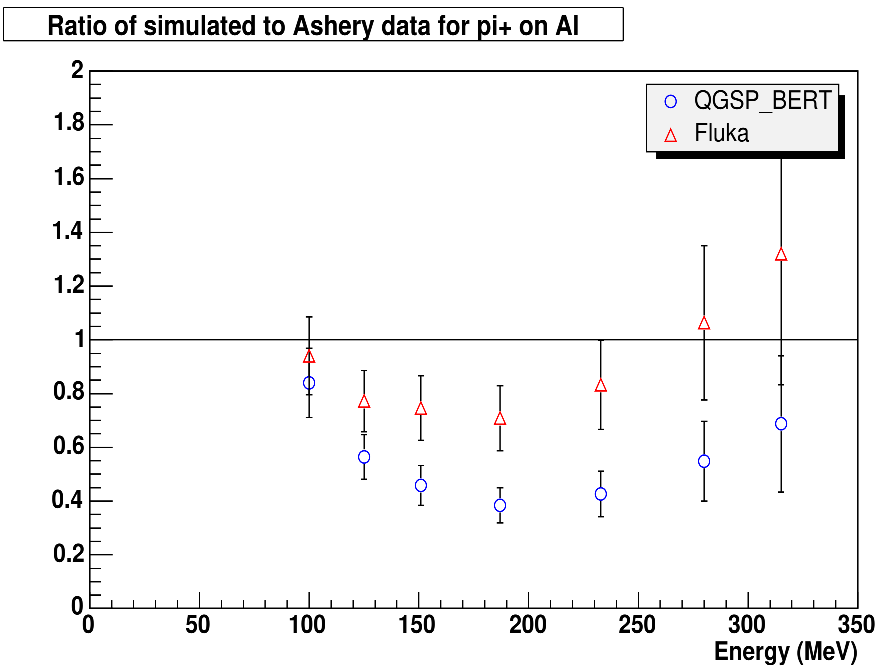

Figure 28: Simulated to experimental (Ashery) total absorption cross section ratio for π^+ on aluminium as a function of energy

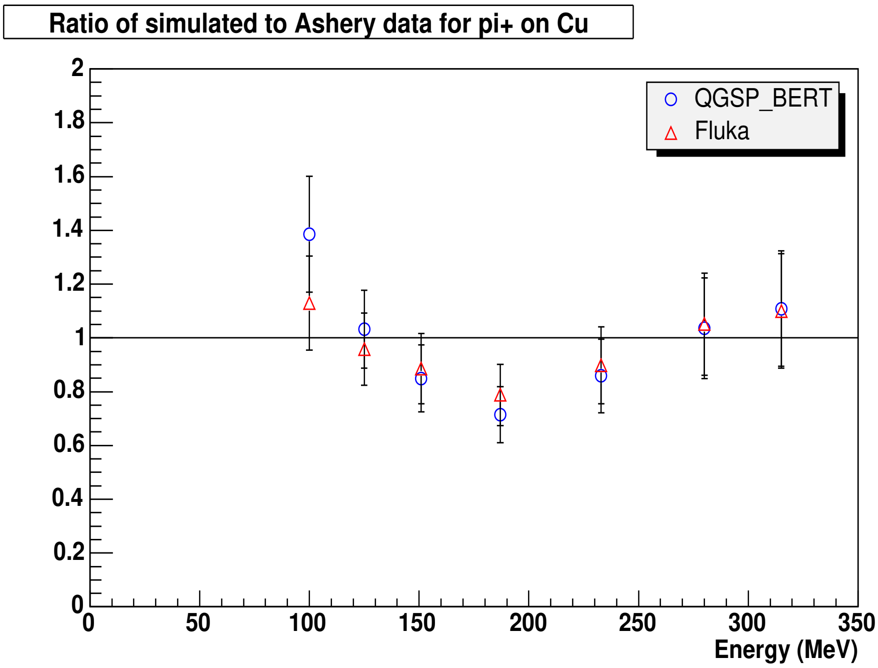

Figure 29: Simulated to experimental (Ashery) total absorption cross section ratio for π^+ on copper as a function of energy

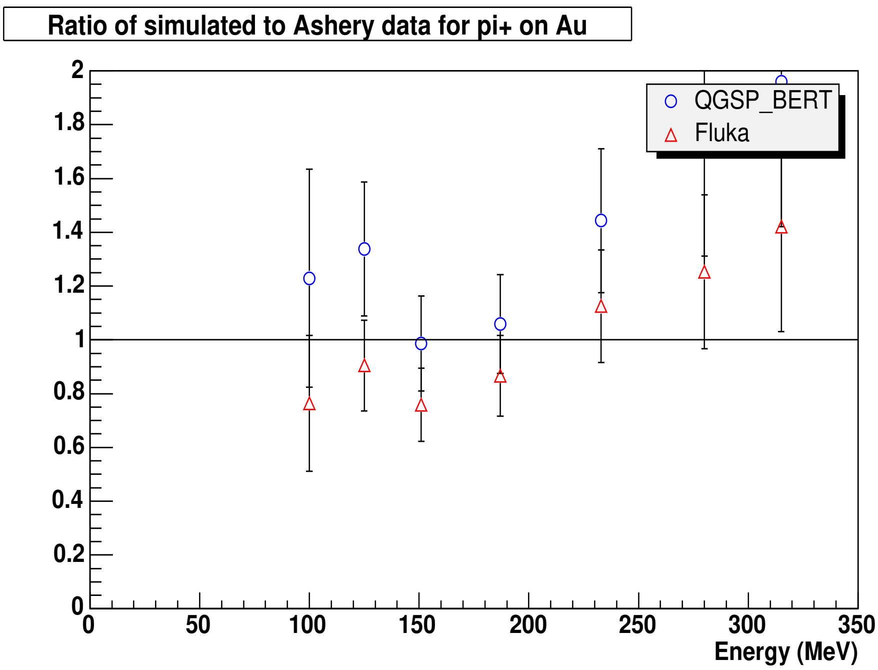

Figure 30: Simulated to experimental (Ashery) total absorption cross section ratio for π^+ on gold as a function of energy

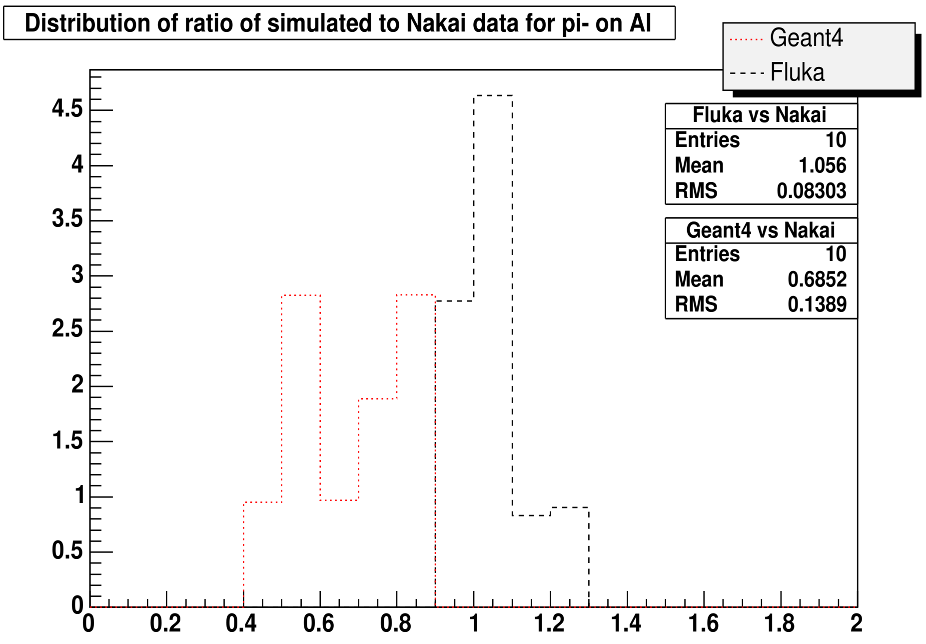

Figure 31: Error-weighted distribution (see Section 4 for more detailed explanation) of simulated to experimental (Nakai) total absorption cross section ratio for π^- on aluminium

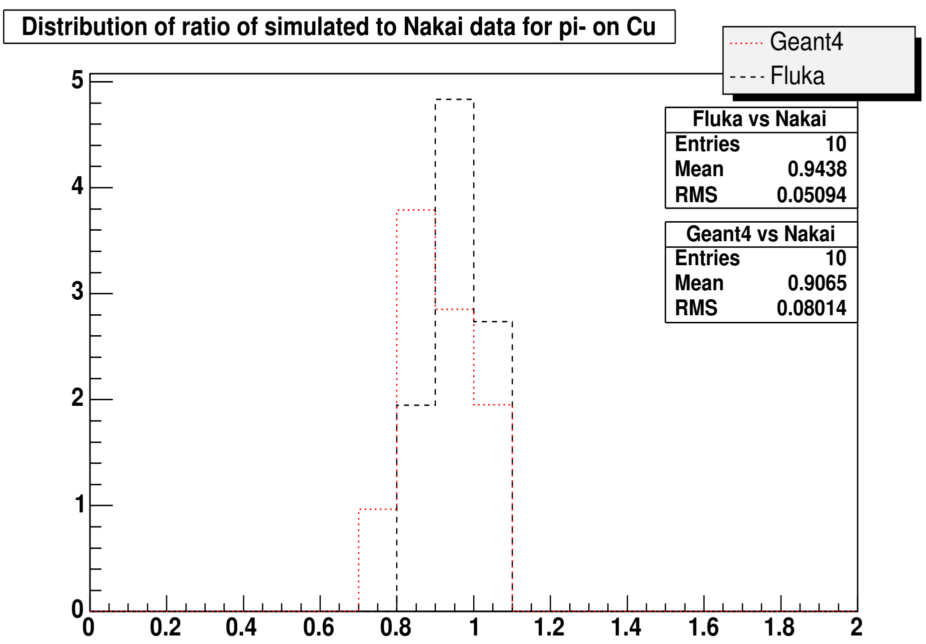

Figure 32: Error-weighted distribution (see Section 4 for more detailed explanation) of simulated to experimental (Nakai) total absorption cross section ratio for π^- on copper

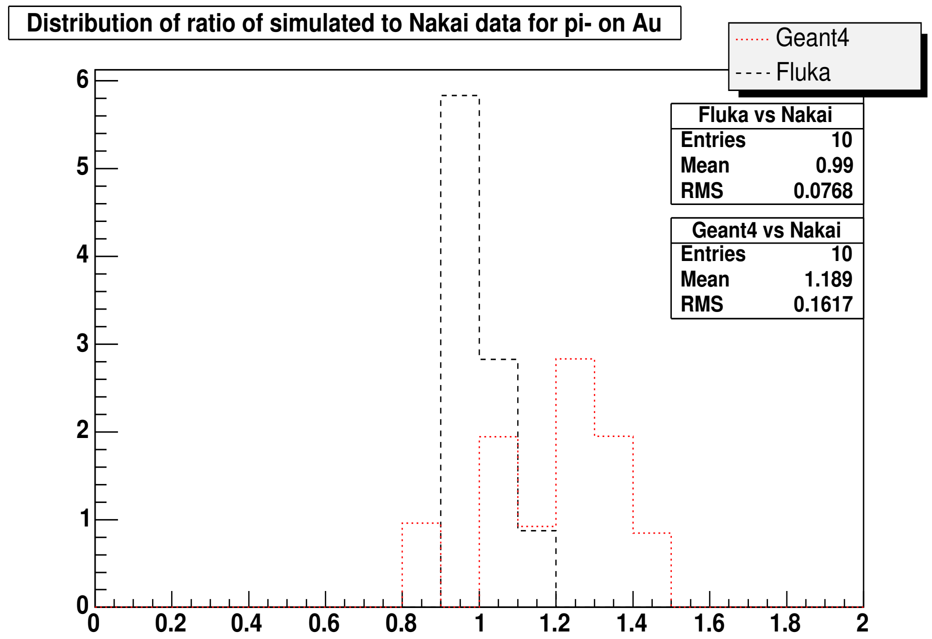

Figure 33: Error-weighted distribution (see Section 4 for more detailed explanation) of simulated to experimental (Nakai) total absorption cross section ratio for π^- on gold

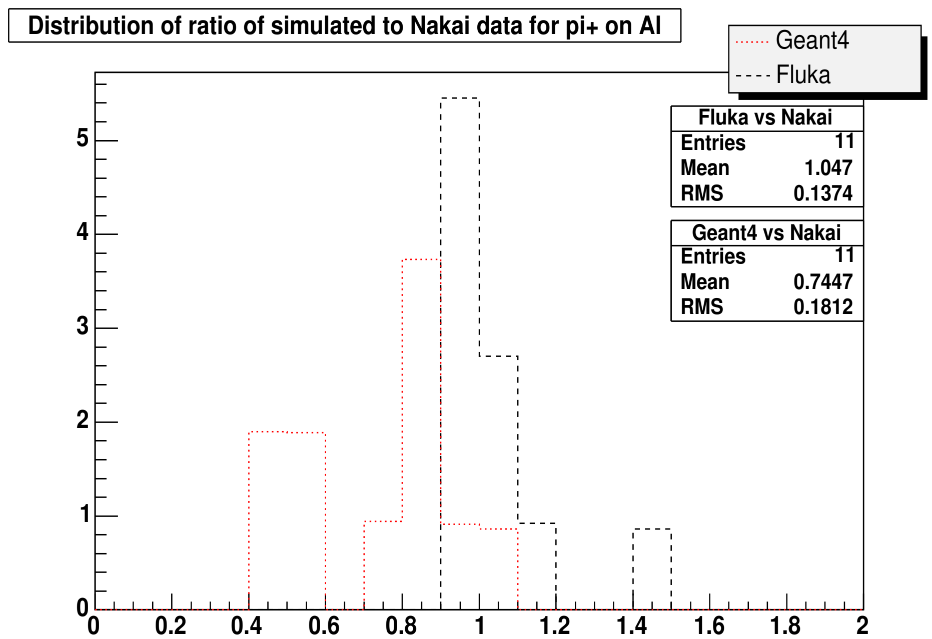

Figure 34: Error-weighted distribution (see Section 4 for more detailed explanation) of simulated to experimental (Nakai) total absorption cross section ratio for π^+ on aluminium

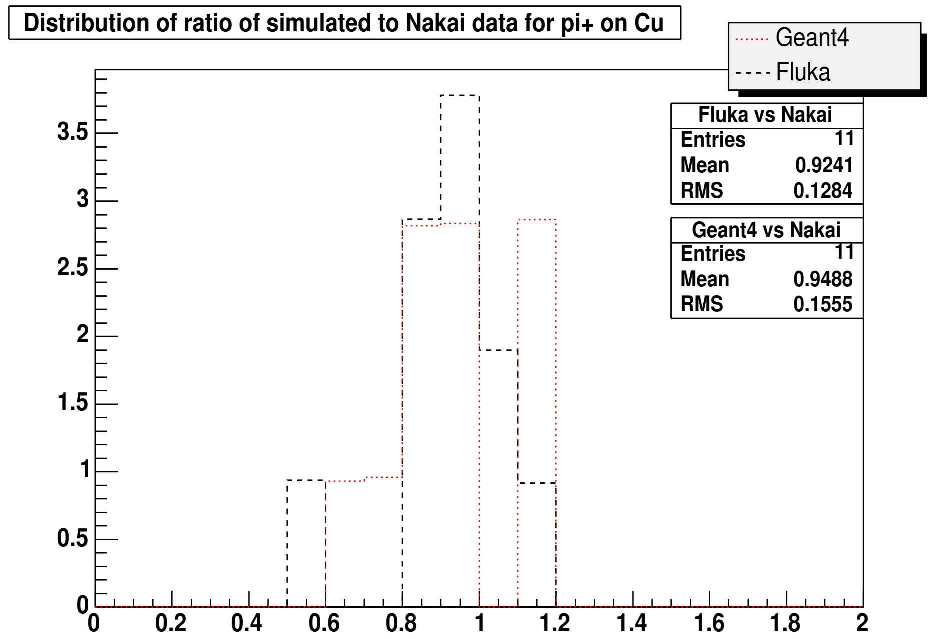

Figure 35: Error-weighted distribution (see Section 4 for more detailed explanation) of simulated to experimental (Nakai) total absorption cross section ratio for π^+ on copper

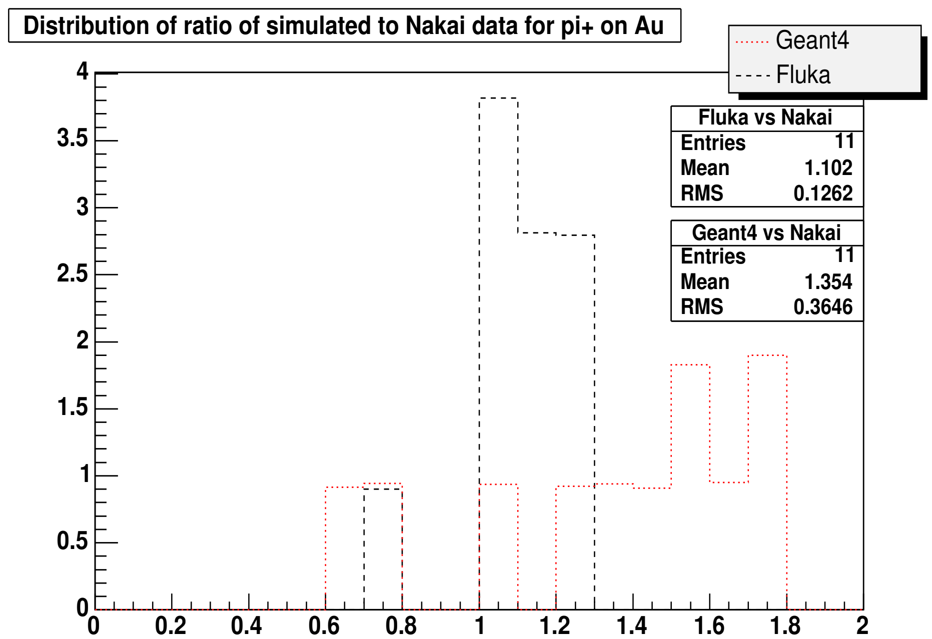

Figure 36: Error-weighted distribution (see Section 4 for more detailed explanation) of simulated to experimental (Nakai) total absorption cross section ratio for π^+ on gold

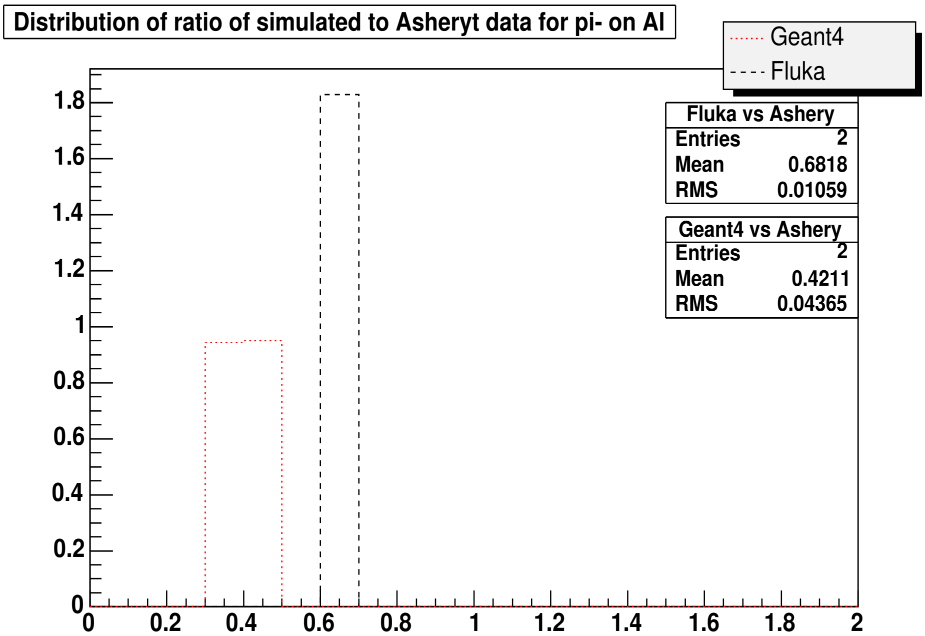

Figure 37: Error-weighted distribution (see Section 4 for more detailed explanation) of simulated to experimental (Ashery) total absorption cross section ratio for π^- on aluminium

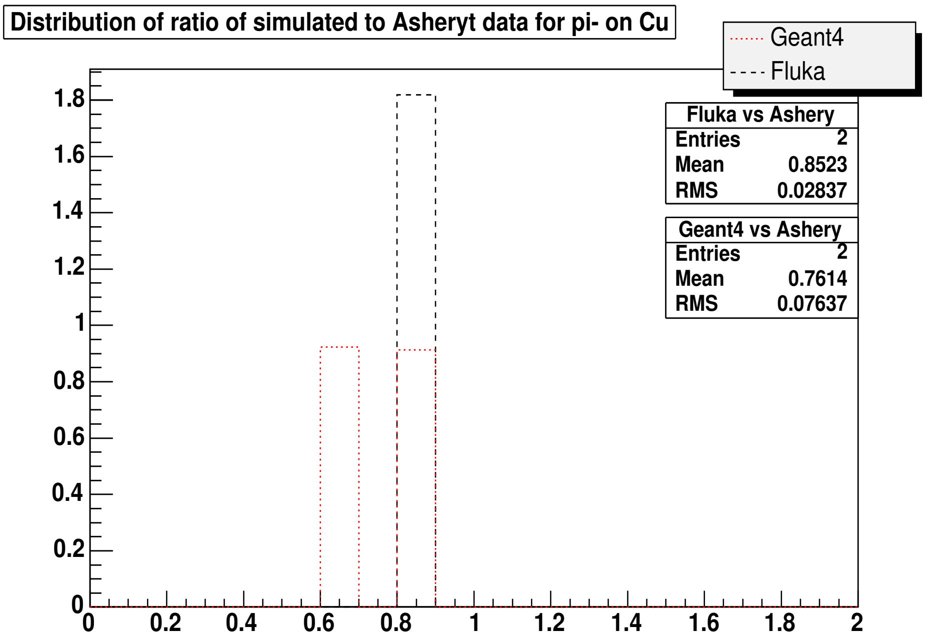

Figure 38: Error-weighted distribution (see Section 4 for more detailed explanation) of simulated to experimental (Ashery) total absorption cross section ratio for π^- on copper

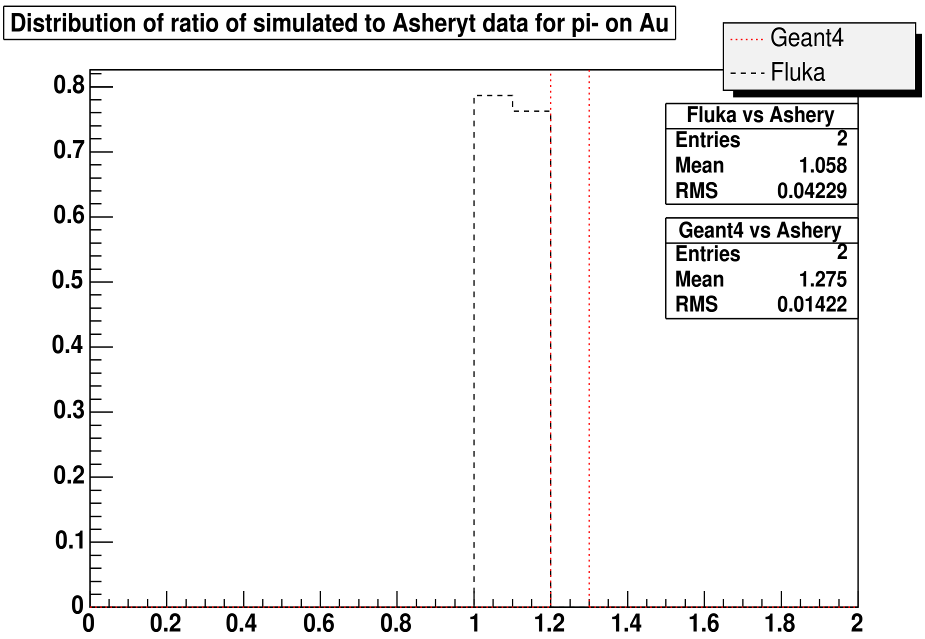

Figure 39: Error-weighted distribution (see Section 4 for more detailed explanation) of simulated to experimental (Ashery) total absorption cross section ratio for π^- on gold

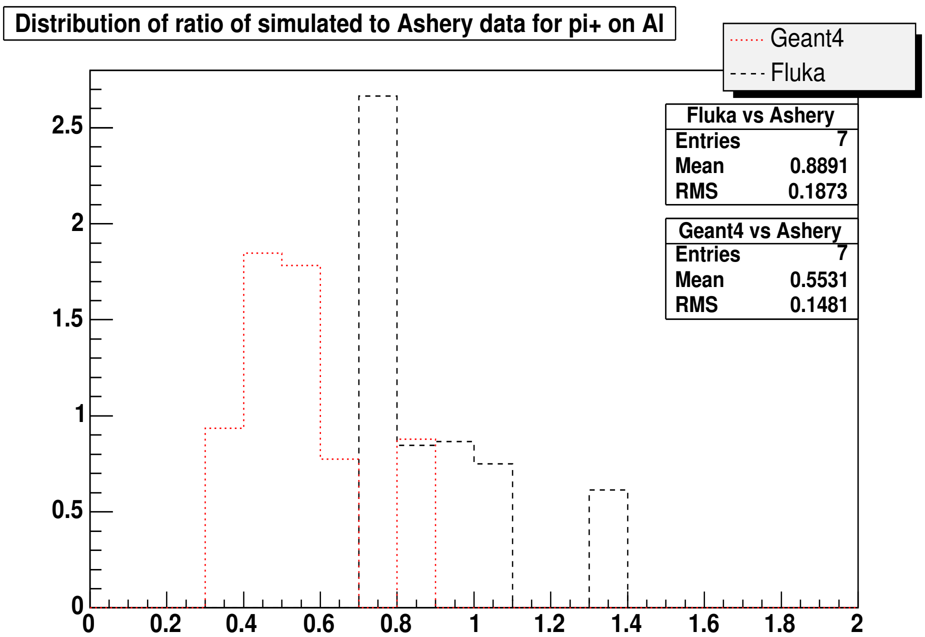

Figure 40: Error-weighted distribution (see Section 4 for more detailed explanation) of simulated to experimental (Ashery) total absorption cross section ratio for π^+ on aluminium

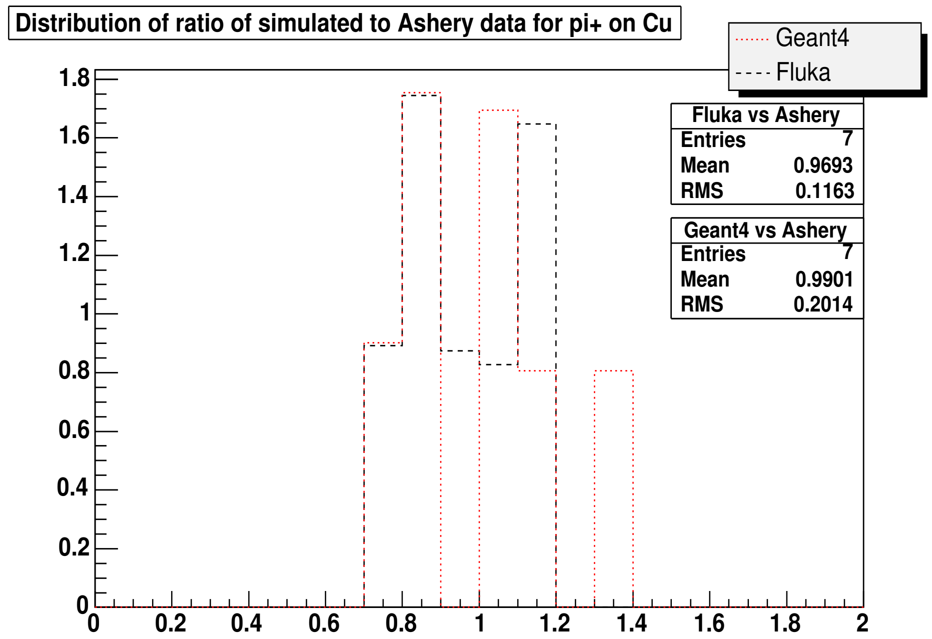

Figure 41: Error-weighted distribution (see Section 4 for more detailed explanation) of simulated to experimental (Ashery) total absorption cross section ratio for π^+ on copper

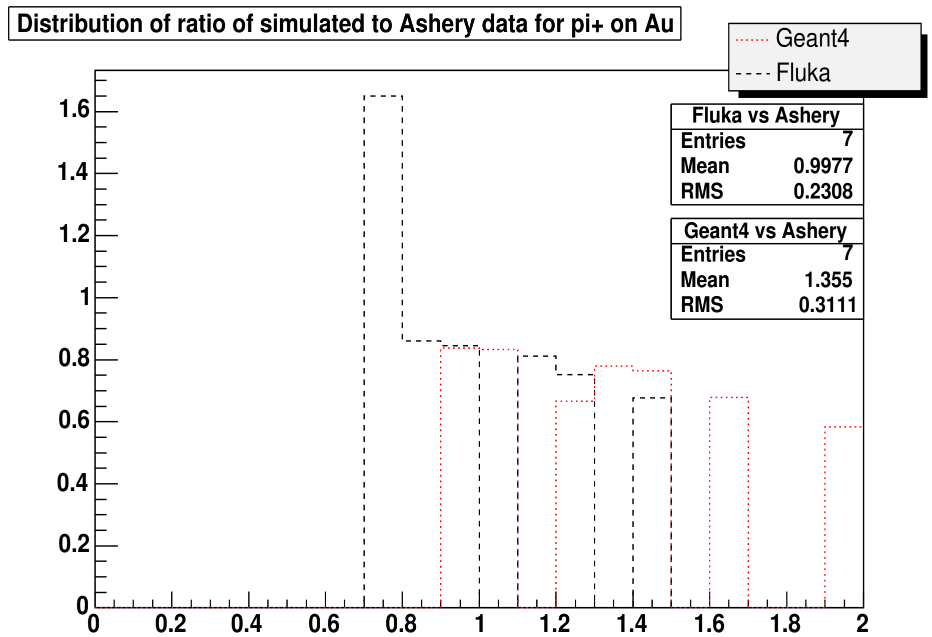

Figure 42: Error-weighted distribution (see Section 4 for more detailed explanation) of simulated to experimental (Ashery) total absorption cross section ratio for π^+ on gold

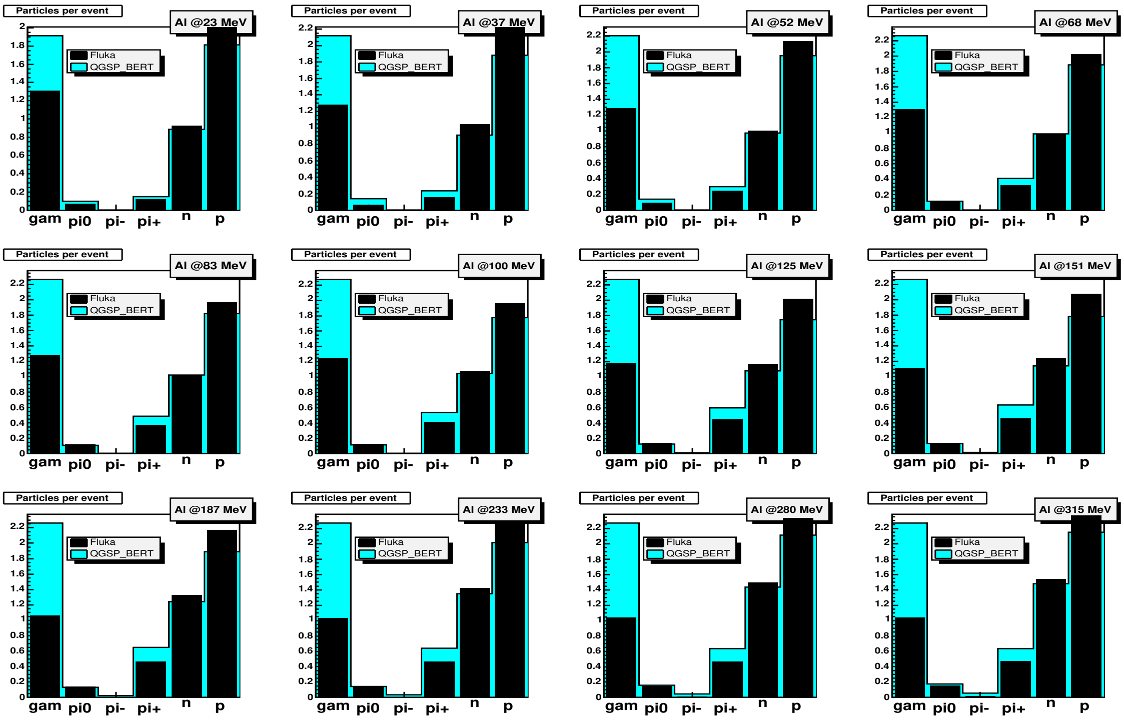

Figure 43: Multiplicity of outgoing particles for π^+ on aluminium

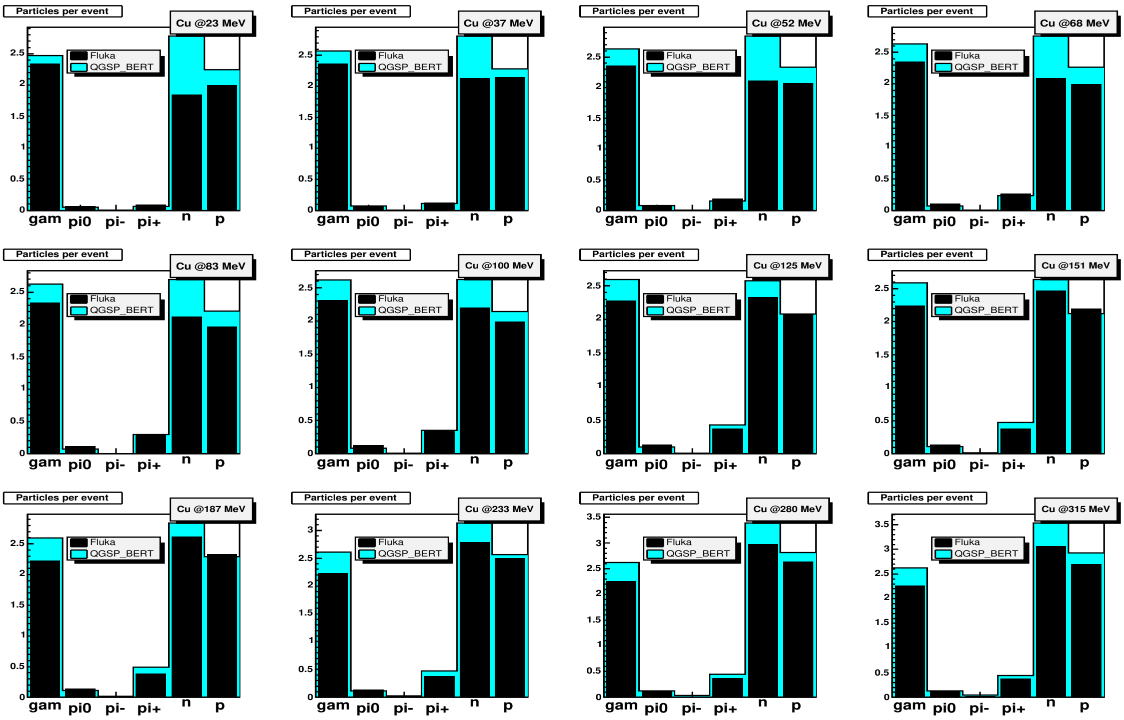

Figure 44: Multiplicity of outgoing particles for π^+ on copper

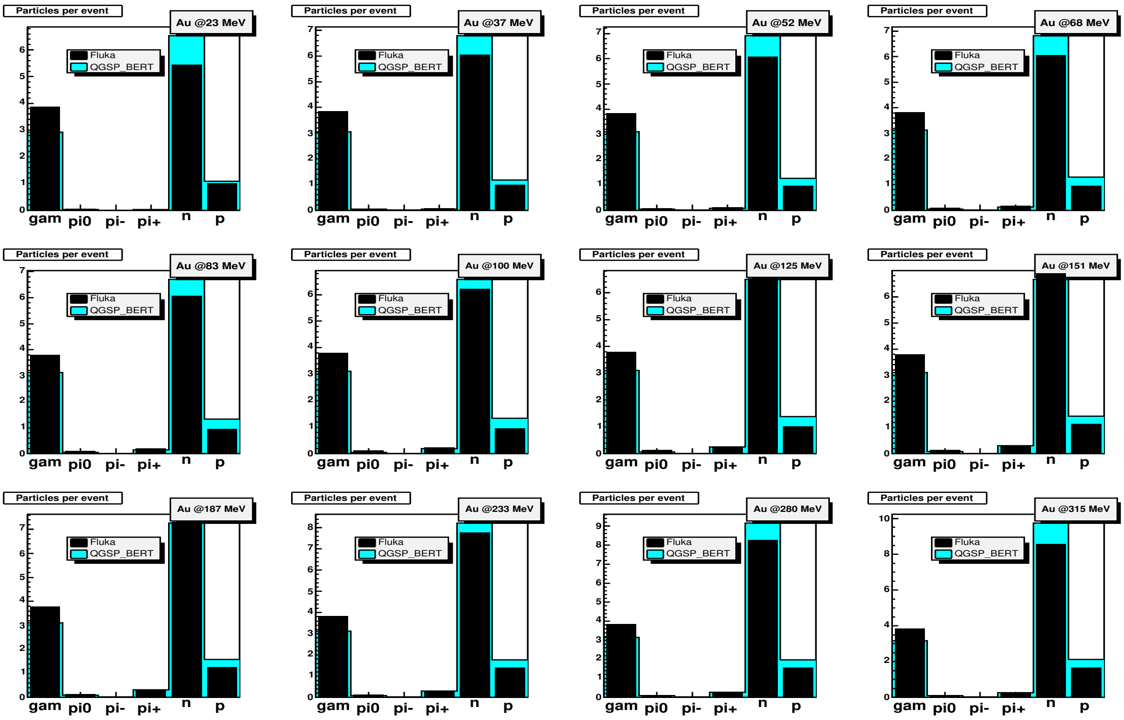

Figure 45: Multiplicity of outgoing particles for π^+ on gold

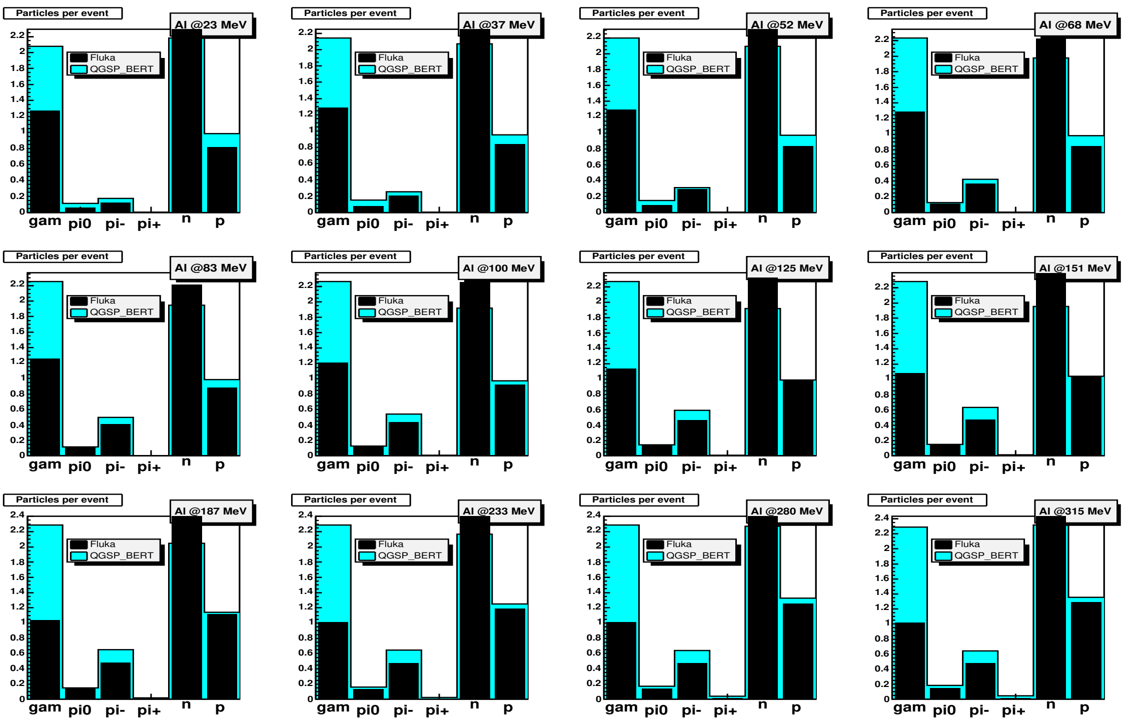

Figure 46: Multiplicity of outgoing particles for π^- on aluminium

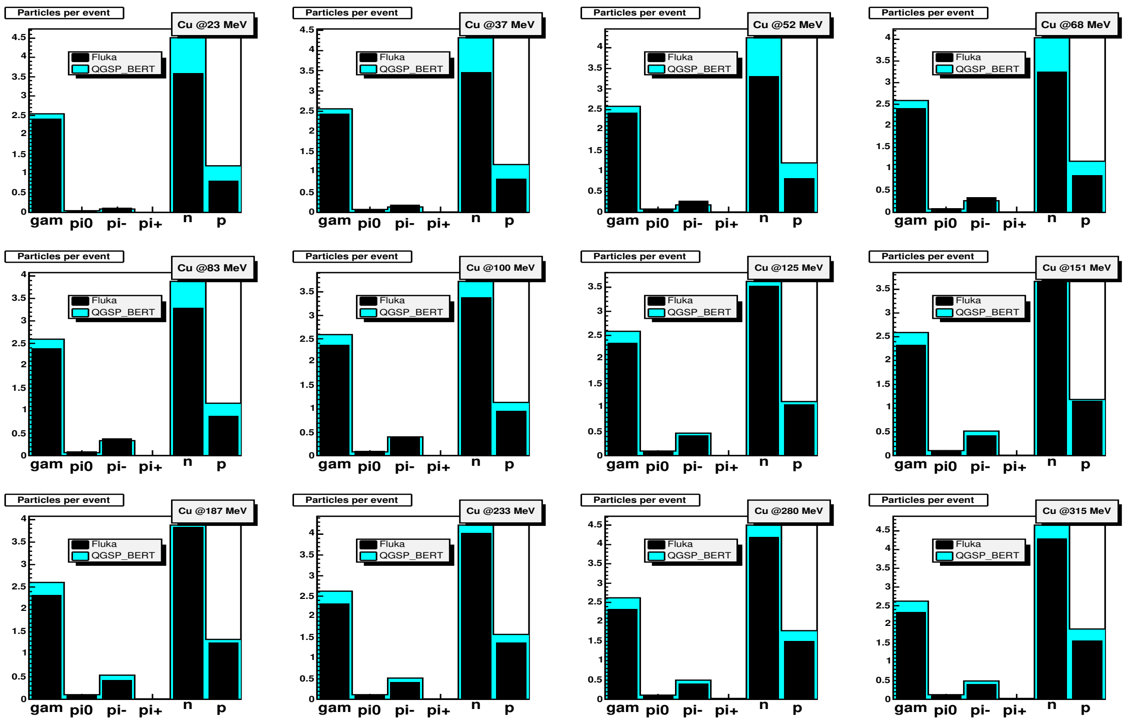

Figure 47: Multiplicity of outgoing particles for π^- on copper

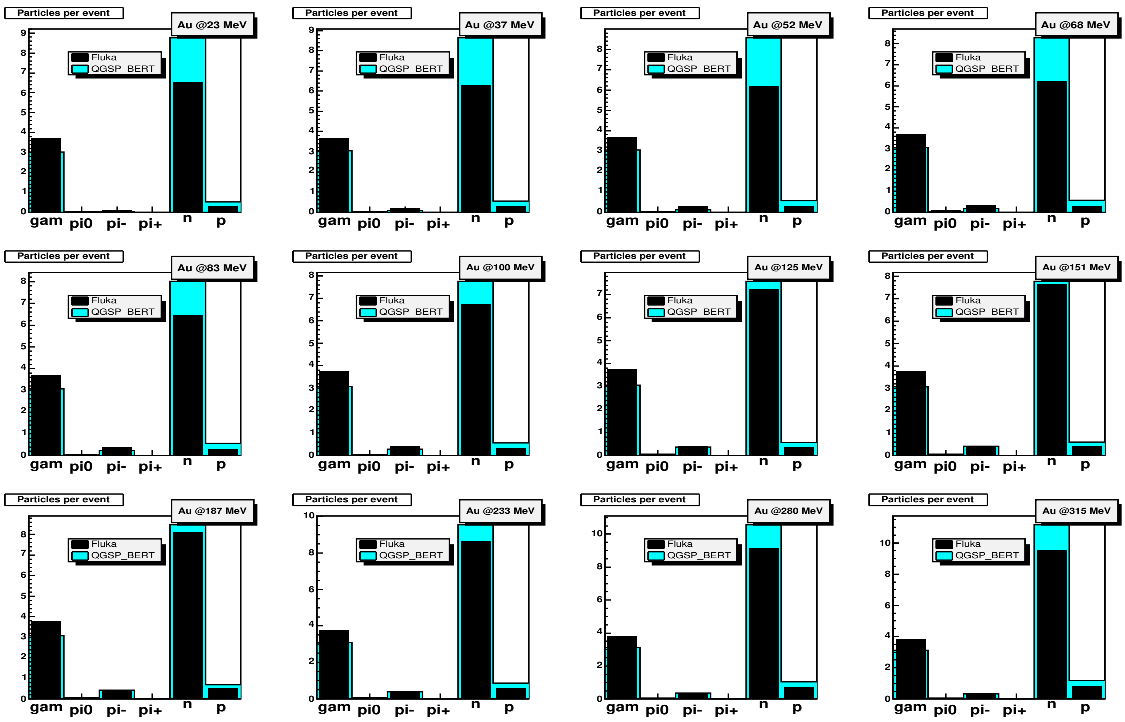

Figure 48: Multiplicity of outgoing particles for π^- on gold

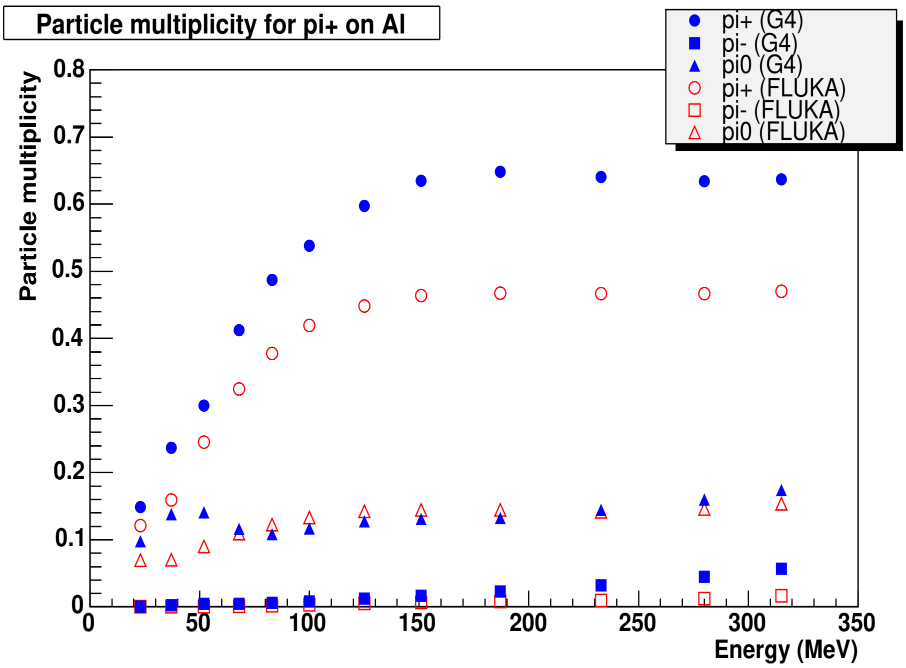

Figure 49: Mutliplicity of outgoing pions as function of energy for π^+ on aluminium

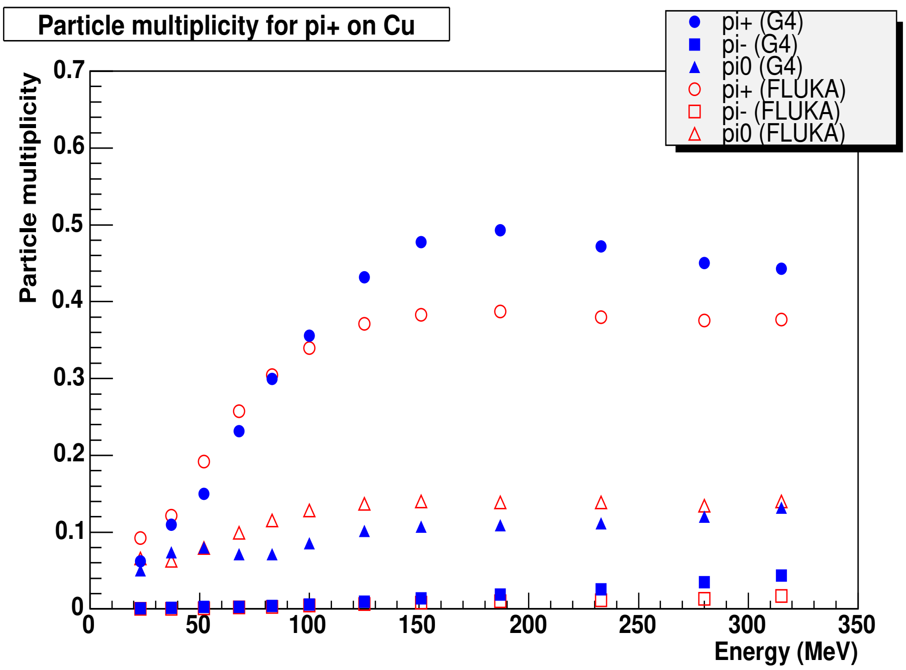

Figure 50: Mutliplicity of outgoing pions as function of energy for π^+ on copper

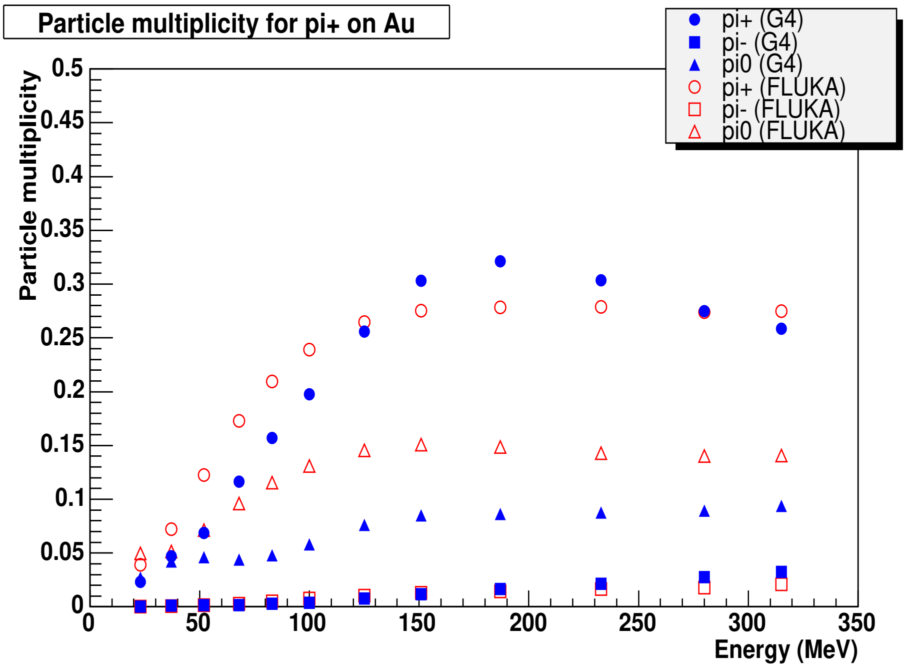

Figure 51: Mutliplicity of outgoing pions as function of energy for π^+ on gold

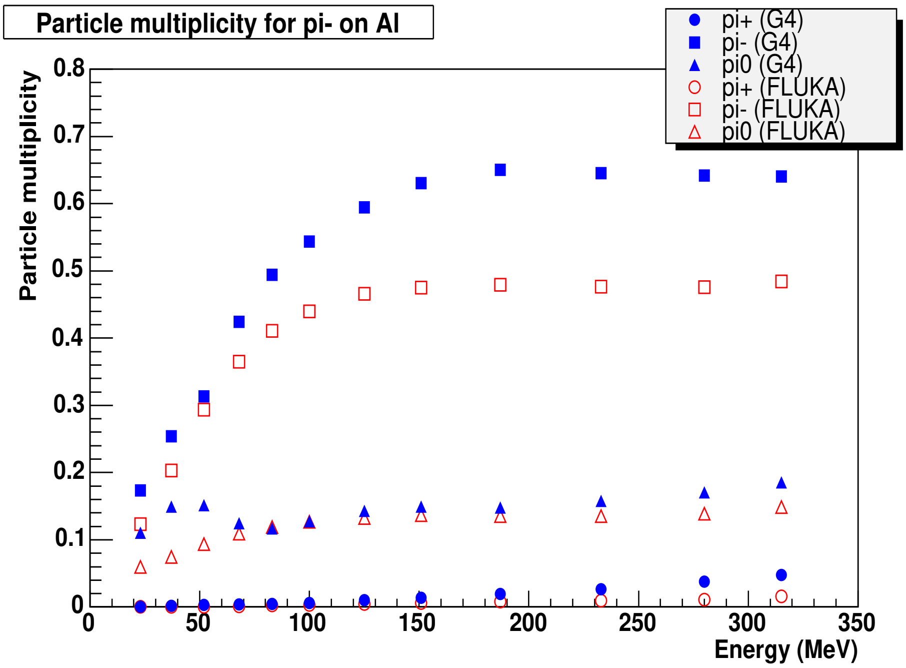

Figure 52: Mutliplicity of outgoing pions as function of energy for π^- on aluminium

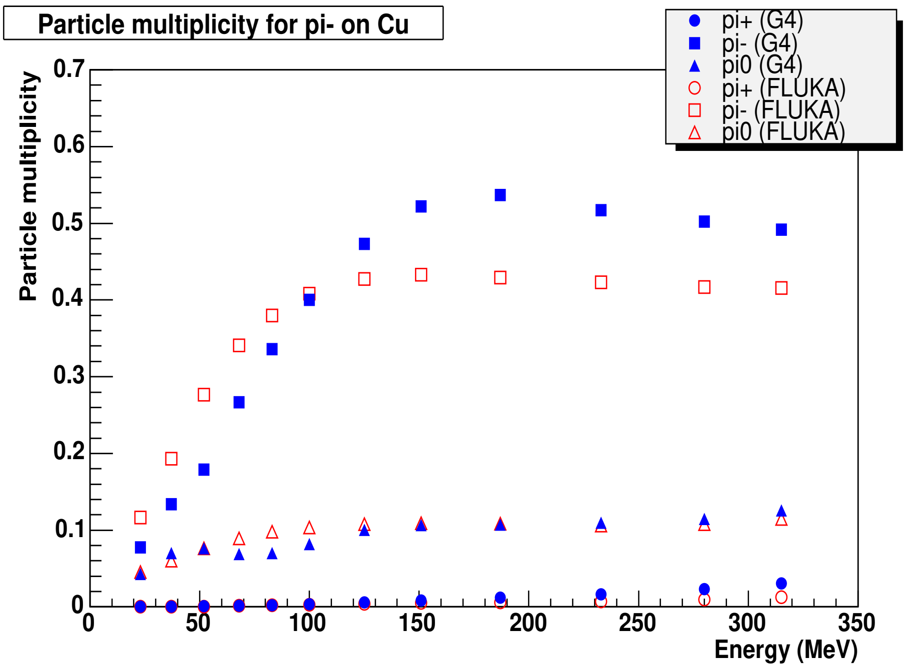

Figure 53: Mutliplicity of outgoing pions as function of energy for π^- on copper

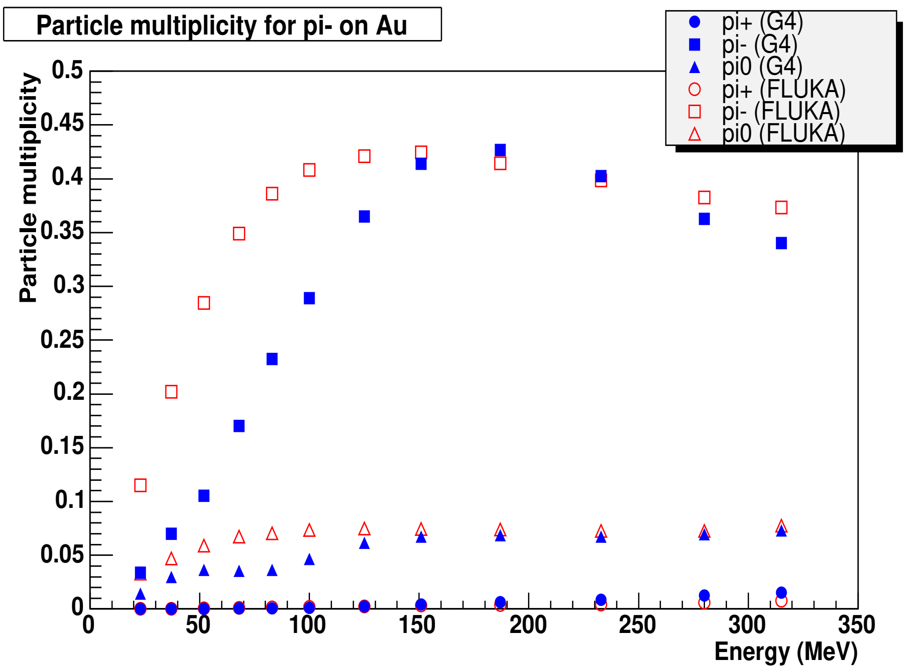

Figure 54: Mutliplicity of outgoing pions as function of energy for π^- on gold